3-26-2020

Mismatched Filter Effects on Synthetic Aperture Radar Image Quality Metrics

Jerrod M. Kempf

MISMATCHED FILTER EFFECTS ON SYNTHETIC APERTURE RADAR IMAGE QUALITY METRICS

THESIS

Jerrod M. Kempf, Capt, USAF

AFIT-ENG-MS-20-M-030

DEPARTMENT OF THE AIR FORCE
AIR UNIVERSITY

AIR FORCE INSTITUTE OF TECHNOLOGY

Wright-Patterson Air Force Base, Ohio

AFIT-ENG-MS-20-M-030

MISMATCHED FILTER EFFECTS ON SYNTHETIC APERTURE RADAR IMAGE QUALITY METRICS

THESIS

Presented to the Faculty

Department of Electrical and Computer Engineering

Graduate School of Engineering and Management

Air Force Institute of Technology

Air University

Air Education and Training Command

in Partial Fulfillment of the Requirements for the

Degree of Master of Science in Electrical Engineering

Jerrod M. Kempf, B.S.E.E.

Capt, USAF

March 26, 2020

AFIT-ENG-MS-20-M-030

MISMATCHED FILTER EFFECTS ON SYNTHETIC APERTURE RADAR IMAGE QUALITY METRICS

THESIS

Jerrod M. Kempf, B.S.E.E.
Capt, USAF

Committee Membership:

Julie A. Jackson, Ph.D
Chair

Richard K. Martin, Ph.D
Member

Maj James R. Lievsay, Ph.D
Member

AFIT-ENG-MS-20-M-030

Abstract

Detection of targets across a wide dynamic range is an enduring challenge in radar. Pulse compression techniques such as matched filtering aid in target detection, but high sidelobes in the response limit the range of detectable targets. This work formulates a modified least-squares mismatched filter that greatly reduces these sidelobes in order to enable the detection of small radar cross section targets in the presence of considerably larger scatterers, increasing the dynamic range. Unlike previous mismatched filters, the proposed filter is applicable to noisy, oversampled signals with no requirements on signal structure. This paper considers the degree of signal oversampling on the filter's performance as well as characterizing sidelobe suppression across a wide spectrum of noise environments. Range profiles and images are presented to demonstrate the superior sidelobe suppression of the modified least-squares mismatched filter in comparison to the commonly employed matched filter. Various weighting vectors are introduced to further increase sidelobe suppression for particular scene geometries. The modified mismatched filter created with the addition of a noise compensation term is shown to have superior sidelobe suppression to that of the matched filter across all signal-to-noise ratios, coming at the relatively low expense of a small degree of mainlobe energy loss and widening, as well as increased processing time.

Table of Contents

Page

List of Figures

List of Tables

MISMATCHED FILTER EFFECTS ON SYNTHETIC APERTURE RADAR IMAGE QUALITY METRICS

I. Introduction

1.1 Problem Statement

Synthetic aperture radar (SAR) systems have seen significant increase in use in recent years because of their ability to work at large stand-off distances and in a variety of low visibility conditions. Detection of relatively small targets has been a recurring challenge in radar systems however because of high sidelobes caused from pulse compression techniques. Because of this, mismatched filters have been a recurring topic of interest due to their low sidelobes in the filter's response. Many works in the past have applied various mismatched filters to pulse-coded radar signals to show this superior sidelobe performance [1–8]. However, previous works have not taken into account the perturbations in the received signal from either radio frequency noise or clutter, nor has the focus been on non-radar optimized waveforms. Radar optimized waveforms and hardware have more control over their signal-to-noise ratio (SNR) and can increase performance by increasing transmit power; an advantage that is not possible in other applications such as passive SAR. This work formulates a mismatch filter approach for general signals in a noisy environment to improve both active, radar optimized applications and passive applications.

1.2 Research Objectives

The goals of this work are twofold:

- Formulate a robust mismatched filter design that is suitable for a general signal of interest in a noisy environment.

- Evaluate the performance of the new mismatched filter design compared to that of the matched filter in various noise and clutter environments.

1.3 Assumptions

The assumptions in this work include:

- The transmitted signals in each scenario are assumed to be band limited and to have no competing signals within their dedicated band. Each simulation consists of only the transmit signal of interest and when applicable, additive noise.

- Each signal can be reconstructed perfectly. This assumption is required for creation of the matched and mismatched filters produced for each pulse used in the image formation. Knowledge of the transmitted signal is inherent in monostatic cases and can be collected from the direct path in passive applications.

- Superposition holds for scenes consisting of multiple scatterers. This assumption allows for filter performance determined on the impulse response to be extended to scenes with multiple scatterers. This is a common assumption that allows for the interaction of the signal in the scene to be modeled as a linear system.

1.4 Contributions

The application of the methods described in this work will:

- Create a more robust least-squares mismatched filter (LSMMF) formulation that allows for filter use in cases of oversampled signals and noisy environments.

- In the presence of additive noise, allow for significantly reduced sidelobes compared to that of the matched filter, thus increasing the detectability of small targets.

- With a priori knowledge of the scene, allow for further suppression of sidelobes using a weighting vector.

1.5 Document Overview

The rest of this thesis is organized as follows: Chapter II gives an overview of the necessary radar fundamentals, as well as introducing orthogonal frequency-division multiplexing (OFDM) signals as the signal of interest in this work. Chapter II continues with an overview on matched and mismatched filtering, the signal processing chain, and introduces the metrics used to evaluate filter performance. Chapter III focuses on describing the modifications to the traditional LSMMF used in this work to allow for a wider use of application. Chapter IV includes the results of the simulations used to characterize the performance of the mismatched and matched filter in various conditions and environments. Finally, Chapter V summarizes the findings of the work as a whole and includes recommendations for future works going forward.

II. Signal Chain and Filtering Essentials

2.1 Chapter Overview

This chapter provides the reader with the necessary framework to understand the concepts and results in the following chapters. To this end, a description of concepts will begin with an overview of SAR fundamentals. Bi-static geometries will be introduced as a means of introducing passive SAR and signals of opportunity, although the filtering methods considered apply to both monostatic and bistatic cases, as well as both active and passive radar modes. A brief overview of OFDM signals will be given since they will be the signals of opportunity used in this work. Next a description of the matched filter and its place in the processing chain as a whole is included. At this point, the reader is provided an overview of the traditional LSMMF including background on its use and advancements over time. Finally, range profiles and images, along with metrics associated with them, are introduced as the means of performance evaluation between different filters.

2.2 SAR Fundamentals

SAR differs fundamentally from traditional radar in that the end product is a two-dimensional intensity image of the scene of interest [9]. A SAR collection in this work will consist of using the phase history collected from successive radar pulses to coherently build up an image via an imaging algorithm. The phase history for each pulse is formed in this work by considering the return signal from a single scatterer and using a radar filter to form a range profile. This range profile, along with details of the simulated scene, is used to generate the simulated phase history for each pulse as described later in this chapter. In this work, backprojection [10] will be the imaging algorithm of choice, though the results in this work are also applicable

to other imaging algorithms.

In traditional SAR, each pulse is emitted from an aircraft towards the scene of interest, where each scatterer will cause a return at a delay proportional to the object's two-way range from the transmitter. Because the radar return delay is dependent on the one-dimensional scatterer range, returns from multiple aspects are required to allow for two-dimensional target positioning.

For a traditional monostatic SAR collection, the slant range resolution, ρ_u, is given by [11]

$$\rho_u = \frac{c}{2B}, \tag{1}$$

where c is the speed of light and B is the bandwidth of the transmitted signal. This result is identical to traditional radar, and is not dependent on the aperture.

2.2.1 Bi-static/Multi-static Geometries

Previously, it was assumed that both the transmitter and receiver were co-located. A more general bi-static case consists of a receiver and transmitter in different locations. In this work, the general case will assume a stationary transmitter and a moving receiver forming the synthetic aperture. Multi-static cases include any collection geometry with multiple transmitters or multiple receivers, with each transmitter/receiver pair forming a bi-static pair. Single bi-static pairs will be the focus throughout this work. An example of a multi-static geometry consisting of two bistatic pairs is seen in Figure 1.

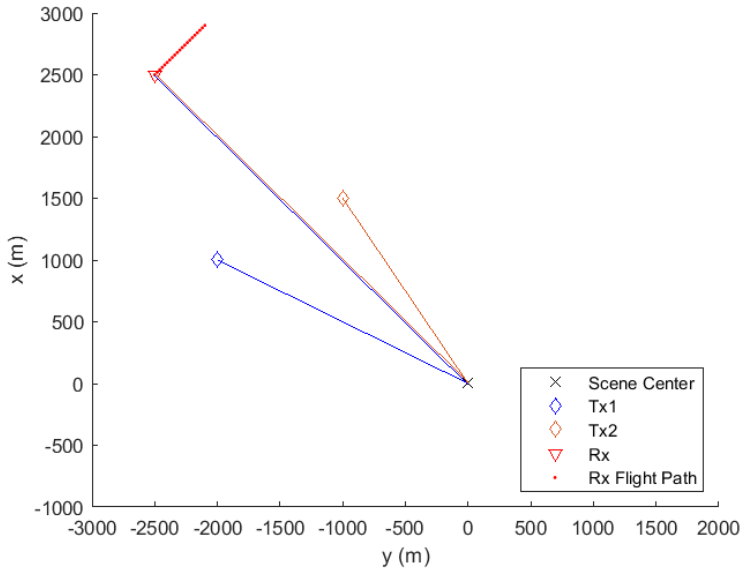

Figure 1: A multi-static geometry consisting of 2 transmitters and 1 receiver.

For a bi-static geometry, the slant range resolution, ρ_u, is given by [11]:

$$\rho_u = \frac{c}{2B\cos\left(\frac{\beta}{2}\right)}, \tag{2}$$

where β is the bi-static angle formed between the transmitter, scene center, and receiver. For a given bi-static pair, the bi-static angle, β, is defined as the angle formed between the vectors connecting the receiver to the scene center and the transmitter to the scene center.

2.2.2 Passive SAR

Passive SAR is a form of SAR in which emitters of opportunity in the environment are used rather than transmitting a dedicated radar signal. The motivation for passive SAR is to make use of existing high power transmitters such as digital television and communication signals as emitters of opportunity. This approach offers a number of desired features such as low probability of intercept, reduced platfor-

m/power requirements, and reduced spectrum congestion [12]. There are drawbacks to this approach however, since the user has no control over the transmitted waveforms. As a result, the user has no control over waveform characteristics such as signal power and bandwidth, which will greatly affect the produced image's resolution and other quality factors. Additionally, passive SAR geometries are inherently bi-static/multi-static, resulting in reduced image resolution and increased geometric complexity. While mismatched filter applications are applicable to both active and passive SAR, the limited control in passive SAR may make a better optimized mismatched filter particularly attractive.

2.3 OFDM Waveforms

OFDM waveforms are commonly used in communication applications. OFDM signals are named such because they are defined in the frequency domain over N discrete subcarriers. Each of the subcarriers are separated in frequency by Δf Hz, resulting in a signal bandwidth of $B = N\Delta f$ Hz. Each of these subcarriers is modulated with a complex value according to a predefined modulation scheme such as quadrature amplitude modulation (QAM) or phase shift keying (PSK). The signal in the frequency domain remains constant for the length of an information symbol defined as $T_s = 1/B$. The OFDM signal parameters used in this work are given in Table 1. OFDM signals are used in this work to indicate that the methods used in this paper are applicable to a wide variety of signals including non-radar optimized waveforms carrying random user data, however the results are extendable to any signal type.

Table 1: Parameters used for OFDM signal generation:

Parameter	Symbol	Value
Number of Subcarriers	N	1024
Carrier Frequency	f_c	728 MHz
Carrier Separation	Δf	15 kHz
Modulation Scheme	–	256 QAM
Bandwidth	B	15.36 MHz

Because the bandwidths of the OFDM signals listed in Table 1 are relatively small when compared to many monostatic SAR systems, the resulting range resolution of images formed from passive SAR is relatively poor.

The parameters used above are meant to be representative of the types of characteristics a signal of opportunity may have. The relatively low bandwidth (in the radar context) of 15.36 MHz was chosen to be representative of an Long-Term Evolution (LTE) signal. The nominal slant range resolution of such a signal in a monostatic case from (1) is on the order of 10 m. Note that an increase of the bandwidth will proportionally increase the resolution regardless of the radar filtering technique used. The choice of all of the above variables does not affect the performance of the filtering techniques presented in the following chapter and are held constant for readability.

This work uses a general bi-static example to more directly show the utility in passive SAR applications, which are inherently bi-static. The bi-static geometry introduces a predictable loss in resolution given in (2) regardless of the radar filtering technique and does not affect the comparison between techniques. Throughout this work, the collection aperture consists of 41 pulses over a span of 2 degrees. The receiver and transmitter are both assumed to be at a constant elevation of 10 degrees with the transmitter being located 30 degrees in azimuth away from the center of

the receiver's flight path. While a bi-static geometry is used as the test example in this work, the results for monostatic cases would yield similar results. Similarly, the choice of OFDM signals is not required and is used to offer a relatively simple and generic signal.

2.3.1 Convolution Matrix

Throughout this work, the linear operator of convolution is used to create filter responses. In radar processing, a received signal, $\mathbf{x}$ is typically convolved with a set of filter coefficients, $\mathbf{h}$, to produce a response, $\mathbf{z}$. Often this relationship is described with the convolution operator $*$ as in

$$\mathbf{z} = \mathbf{x} * \mathbf{h}. \tag{3}$$

The convolution required in (3) can be implemented through matrix multiplication as well which is more convenient when matrix algebra tools are used for processing. If $\mathbf{x}$ is of length N, and is to be convolved with $\mathbf{h}$ which is also of length N, then the convolution matrix, $\mathbf{\Theta}_x$, of $\mathbf{x}$ is a $2N-1 \times N$ matrix. The first column of $\mathbf{\Theta}_x$ are the N entries of $\mathbf{x}$ followed by $N-1$ zeros. Each column after the first is the previous column linearly shifted down by 1. As an example, the convolution matrix for a length 4 signal is

$$\mathbf{\Theta}_x = \begin{bmatrix} \mathbf{x}_1 & 0 & 0 & 0 \\ \mathbf{x}_2 & \mathbf{x}_1 & 0 & 0 \\ \mathbf{x}_3 & \mathbf{x}_2 & \mathbf{x}_1 & 0 \\ \mathbf{x}_4 & \mathbf{x}_3 & \mathbf{x}_2 & \mathbf{x}_1 \\ 0 & \mathbf{x}_4 & \mathbf{x}_3 & \mathbf{x}_2 \\ 0 & 0 & \mathbf{x}_4 & \mathbf{x}_3 \\ 0 & 0 & 0 & \mathbf{x}_4 \end{bmatrix}. \tag{4}$$

Using the convolution matrix, (3) can be rewritten using a matrix multiplication as

$$\mathbf{z} = \mathbf{\Theta}_x \mathbf{h}. \tag{5}$$

This matrix multiplication method using the convolution matrix will be used throughout this work for filter application.

2.4 Matched Filtering

The matched filter is widely used across radar applications because of its easy implementation and performance in the presence of noise. The matched filter however, does have relatively high sidelobes which results in poor performance at identifying small scatterers in a scene. For a given time-domain signal $s(t)$, the matched filter coefficients, $\mathbf{h}_m$, are defined as the conjugate of the time reversed values of the signal, i.e., $\mathbf{h}_m$ is samples of $s^*(-t)$ [9]. The application of this filter is analogous to taking the autocorrelation of the signal.

In general, a range profile is formed from the matched filter by convolving the sampled radar return signal, $\mathbf{x}$, with the filter coefficients as in

$$\mathbf{z}_m = \mathbf{x} * \mathbf{h}_m \tag{6}$$

$$\mathbf{z}_m = \mathbf{\Theta}_x \mathbf{h}_m. \tag{7}$$

For a single point scatterer at scene center with reflectivity equal to 1, the return signal, $\mathbf{x}$, is simply the samples of the transmitted signal, $s(t)$, and the filter response, $\mathbf{z}_m$, in this case is called the impulse response.

Because the impulse response of the matched filter is essentially an autocorrelation of the transmitted signal with itself, it will have a predictable structure with a peak in the center of the response and a sidelobe structure that is dependent on the nature

of the transmitted signal. The impulse response is a useful tool to compare filter techniques because simple metrics can be used to compare filtering techniques as will be described later in this chapter.

For a general scene where multiple targets exist at various ranges around the scene center, the return signal prior to sampling, $x(t)$, is instead samples of delayed versions of $s(t)$ scaled by a different magnitude dependent on each scatterer's reflectivity. This relationship can be described as

$$x(t) = \sum_{i=1}^{n} A_i s(t - t_i), \tag{8}$$

where n is the number of scatterers, A_i is the reflectivity of the ith scatterer, and t_i is the time delay corresponding to the differential range of the ith scatterer from scene center. Note that the impulse above in (7) results when there is a single scatterer with zero time delay from scene center and a reflectivity of 1. Most of the analysis in Chapter IV is performed with a single scatterer at scene center, although some multi-target cases are also presented.

2.5 Signal Processing Chain

This section describes the general processing flow given a general return signal defined in (8). The return signal is assumed to be brought down to baseband prior to the processing flow described below. The end result of this processing is to create the phase history to feed into an image formation algorithm. For an OFDM signal with N subcarriers, the Nyquist sampling rate is $\frac{1}{B}$ and produces a sampled return signal $\mathbf{s}$ consisting of N samples. In this work, oversampling is typically used where the sampling rate is instead $\frac{K}{B}$, producing a sampled return signal $\mathbf{s}$ consisting of NK samples, where K is the oversampling rate. In examples where noise is considered,

a noise vector $\mathbf{n}$ is added to the return signal at this point. Note that this return signal corresponds to a single pulse of the aperture and is approximated to occur at a specific azimuth and grazing angle using a move-stop-move approach.

At this stage, a filter (commonly the matched filter or the mismatched filter defined later in this work) is applied to the return signal using (5) resulting in a range profile, $\mathbf{z}$, for the given pulse consisting of $2NK-1$ samples of which the center NK samples, denoted as $\tilde{\mathbf{z}}$, are used for further processing.

The phase history for the pulse can then be represented by

$$\mathbf{G} = \mathbf{G}_{iso} \circ \mathcal{F}\{\tilde{\mathbf{z}}\}, \tag{9}$$

where $\mathbf{G}_{iso}$ is the ideal phase history of the scene of point scatterers and $\circ$ denotes a Hadamard product. For a given scene consisting of i scatterers, the ideal phase history can be described by

$$\mathbf{G}_{iso} = \sum_i A_i \exp\left(j2\pi \mathbf{f} t_i\right), \tag{10}$$

where t_i is the differential time delay of each scatterer from scene center and $\mathbf{f}$ is the vector of sampling frequencies. The differential range, $u_i = ct_i$, of each scatterer for a given pulse is given by the far field approximation

$$\begin{aligned} u_i \approx\ & x_i(\cos\phi_t \cos\psi_t + \cos\phi_r \cos\psi_r) \\ & + y_i(\sin\phi_t \cos\psi_t + \sin\phi_r \cos\psi_r) \\ & + z_i(\cos\psi_t + \cos\psi_r), \end{aligned} \tag{11}$$

where ϕ_t and ψ_t are the azimuth and grazing angle of the transmitter for the given pulse, ϕ_r and ψ_r are the azimuth and grazing angle of the receiver for the given pulse,

and x_i, y_i, and z_i, are the Cartesian coordinates of the ith scatterer with respect to scene center.

Then the phase history, $\mathbf{G}$, of a given pulse encodes the scatterers in the scene and is of length NK.

2.5.1 Noise Modeling

Several sources of noise are possible in a SAR collection. The first possible source is noise from the transmitter, $n_t(t)$, which is transmitted alongside the desired signal $s(t)$. Another source is interference noise, $n_i(t)$, originating from another location. A third possible noise source is receiver noise, $n_r(t)$. With these sources considered, the return signal can be modeled as

$$x(t) = \sum_{i=1}^{n} A_i \left(s(t - t_{1_i}) + n_t(t - t_{1_i}) + n_i(t - t_{2_i}) \right) + n_r(t), \tag{12}$$

where t_{1_i} and t_{2_i} are delays associated with the differential range between scatterers and the transmitter and interference source respectively. Note that the transmitter noise and interference noise are scene dependent with delays dependent on their location relative to the scatterers, whereas the receiver noise is independent of the scene. In practice, filters are designed based on a single scatterer, so it is more relevant to consider the effects of noise with a single scatterer at scene center. This assumption is equivalent to assuming that $\mathbf{G}_{iso} = \mathbf{1}$, and (12) reduces to

$$x(t) = s(t) + n_t(t) + n_i(t) + n_r(t) \tag{13}$$

$$x(t) = s(t) + n(t). \tag{14}$$

Assuming that each term in (13) is uncorrelated allows for a total noise power, P_n, to be computed as a simple sum of the individual noise source powers, $P_{n_t} + P_{n_i} + P_{n_r}$.

Similarly, because there is no scatterer location dependence, the noise's source is no longer relevant, only its statistics. In this work, each noise source is simulated as additive white Gaussian noise and is added directly to the transmit signal for simplicity. The particular distribution of each noise source is not important however, as long as each source is uncorrelated from each other and the desired signal. Because this work relies on superposition holding for scatterers, this noise model also extends to multi-scatterer scenarios.

2.5.2 Phase History Windowing

Phase history windowing is an additional technique that can be used to reduce sidelobes in both the range profile and image domain. To apply this windowing to the range dimension, the phase history corresponding to each pulse needs to be scaled by a set of window coefficients as in

$$\mathbf{G}_{win} = \mathbf{G} \circ \mathbf{w}, \tag{15}$$

where $\mathbf{w}$ is a length NK window. A similar windowing process can also be performed in the cross-range dimension, however such effects are beyond the scope of this work. Comparisons of sidelobe suppression due to the proposed filtering technique and phase history windowing are compared in Chapter IV.

2.6 Backprojection Algorithm Overview

With the phase history, $\mathbf{G}$, of a given pulse, the backprojection algorithm can be used for image construction. The backprojection algorithm begins with applying an inverse Radon filter to the phase history and then zero-padding the result to a large degree on both sides. After zero-padding, an inverse Fourier Transform is used to generate range profiles that are upsampled by a significant factor, typically 100 or

more [10]. In this work, the upsampling factor used is such that the produced range profiles have a factor of 128 more samples than would be produced with Nyquist sampling. Note that these additional samples do not represent an increase in resolution, but merely allow for more precise interpolation onto an image grid. The effect of each pulse across the aperture is added coherently to the appropriate grid points in the image until the entire aperture has been summed.

2.7 Mismatched Filters

Mismatched filters are not a new concept and have appeared in literature since at least the 1960s. The primary goal of a mismatched filter is to reduce sidelobes in the filter response. The matched filter is known to maximize the signal-to-noise ratio (SNR) of the response at the target location, however it also brings with it relatively high sidelobes [9]. In the radar context, the sidelobes of a larger target can obscure the returns of a smaller target, reducing detectability. Mismatched filters seek to reduce these sidelobes at the cost of mainlobe energy.

2.7.1 Least-Squared Mismatched Filter Definition

The mismatched filter focused on in this work is a least-squares mismatched filter (LSMMF). The ideal impulse response at the filter output, $\mathbf{z}_i$, of a Nyquist sampled signal has a peak return at zero delay, with values of zero at all other delays. Such a response would result from

$$\mathbf{z}_i = \mathbf{\Theta}_s \mathbf{h}_i \tag{16}$$

where $\mathbf{\Theta}_s$ is the convolution matrix of the time signal $\mathbf{s}$ and $\mathbf{h}_i$ are the ideal filter coefficients. For a general signal $\mathbf{s}$, there are no coefficients that satisfy this response.

However, a mismatched filter with coefficients $\mathbf{h}_l$ can be computed such that

$$\mathbf{h}_l = \arg\min ||\mathbf{z}_i - \mathbf{\Theta}_s \mathbf{h}||^2, \tag{17}$$

where $\mathbf{h}$ denotes possible filter coefficients. That is, the mismatched filter coefficients are designed such that the mean squared error between the mismatched filter response $\mathbf{z}_l = \mathbf{\Theta}_s \mathbf{h}_l$ and the ideal filter response $\mathbf{z}_i$ is minimized. The form of this minimization is the well known ordinary least-squares result [4]

$$\mathbf{h}_l = (\mathbf{\Theta}_s^H \mathbf{\Theta}_s)^{-1} \mathbf{\Theta}_s^H \mathbf{z}_i, \tag{18}$$

where ^{H} denotes the conjugate transpose. Note that the columns of a convolution matrix are always linearly independent, therefore the inverse in (18) always exists. While (18) offers a simple expression for an alternate filter, it does not take into account the noise environment in any way, nor does the definition of $\mathbf{z}_i$ as an impulse allow for the flexibility of higher sampling rates. These issues will be tackled in Chapter III.

2.7.2 Inclusion of a Weighting Vector

Previously, (18) offered a solution to reducing the mean-squared error between the ideal response and a realizable response across the full range profile. In practice, it is possible that the reduction of the response at a subset of specific delays is more desirable than at others. To this end, a diagonal weighting matrix can be inserted to increase the associated cost of having an undesirable response at specific delays. For example, the response may include delays corresponding to ranges far outside the scene size of interest. In this case, a rectangular window can be used as a weighting vector such that delays corresponding to ranges outside of the window of interest do

not contribute to the least-squares cost function. This allows for further minimization of the sidelobes within the desired window, at the cost of a less desirable response outside the area of interest. The diagonal weighting matrix, $\mathbf{W}$, can be applied using [4]

$$\mathbf{h}_l = (\mathbf{\Theta}_s^H \mathbf{W} \mathbf{\Theta}_s)^{-1} \mathbf{\Theta}_s^H \mathbf{W} \mathbf{z}_i. \tag{19}$$

Note that $\mathbf{W}$ is a $2NK - 1 \times 2NK - 1$ diagonal matrix whose values along the diagonal correspond to the cost weightings associated with the $2NK - 1$ values in the LSMMF filter response, $\mathbf{z}_l$. Uniform weighting in which $\mathbf{W}$ is an identity matrix is generally used in this work; however, examples including rectangular weighting vectors are also presented in Chapter IV.

2.7.3 Other Relevant Research

LSMMFs have a long history and have progressed significantly in application and scope over the decades. Also referred to as a Wiener filter, the LSMMF first saw practical use in the 1960s as a pulse compression technique for interpreting seismic events [13]. The following decade saw LSMMFs being used in the field of radar, where filter coefficients for Barker sequences were tabulated for use to prevent the relatively high sidelobes that occur from autocorrelation [1]. The computational requirements of computing the LSMMF coefficients made application of the filter to a generic signal unappealing however and most published papers focus on pulse-coded signals.

In recent years however, renewed interest in LSMMFs has emerged, including applications to FM signals [8] and multistatic geometries [7]. Currently, various LSMMF designs are also being considered to help mitigate radar processing issues such as range straddling [8] and range sidelobe modulation [14]. While this work focuses primarily on improving detection of small targets in noisy environments, LSMMFs show the potential to help address many modern radar processing issues.

2.8 Impulse Response and Range Profiles

In general, the response of a filter is given by the convolution of a signal of interest with the filter as seen in (3). In the case of a single point scatterer at scene center, this response is defined as the impulse response of the filter as described previously. For a more complex scene, the return signal will consist of several superimposed copies of the signal, each with their own delay and attenuation dependent on their range from the transmitter/receiver pair as seen in (8). The result of convolving this more complex return signal with a given filter forms a range profile for the more complex scene.

Impulse responses will be used throughout this work as a product to display the performance of the matched filter compared to that of the modified LSMMF (MLSMMF) introduced in Chapter III. Because image formation requires a very dense range profile, the upsampled version of the range profile, $\bar{\mathbf{z}}$, is used for illustration and is also used for calculation of the metrics described later in this section. A close up of an example impulse response for a matched and mismatched filter pair is shown in Figure 2. Each filter response depiction also includes a location and reflectivity of the scatterers used in the scene denoted by magenta diamonds.

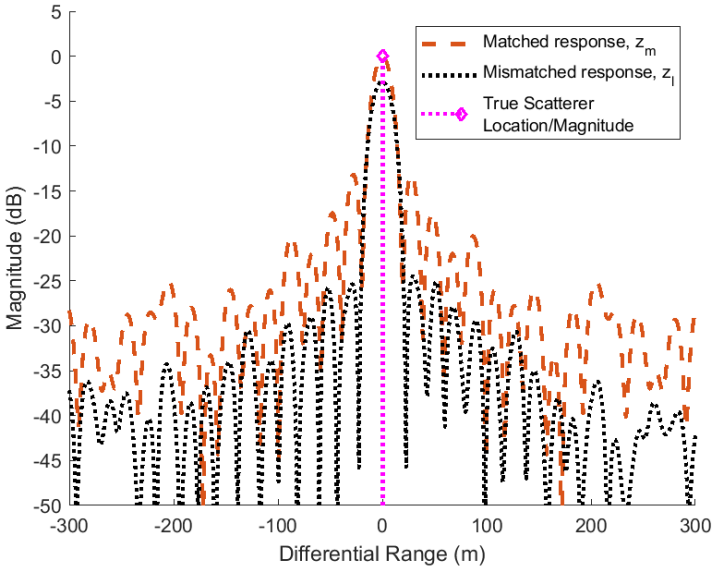

Figure 2: An example impulse response of a matched filter and MLSMMF.

Objective measures of the impulse response that will be used to quantify results include the mismatch loss and integrated sidelobe ratio (ISLR). The mismatch loss of the mismatched filter can be defined as

$$\mathrm{L_{IR}} = 20\log(\max(|\bar{\mathbf{z}}_m|) - \max(|\bar{\mathbf{z}}_l|)), \tag{20}$$

where $\bar{\mathbf{z}}_m$ and $\bar{\mathbf{z}}_l$ are the upsampled ranged profiles of the matched and mismatched filters respectively. The mismatch loss is a measure of the peak power reduction seen in the LSMMF relative to the matched filter. Depending on hardware sensitivity, a large amount of mainlobe loss may force signals below the minimum detectable power level or may lead to increased quantization error. In most cases however, mismatch loss is on the order of 0 to 3 dB and represents only a small loss in peak power.

The ISLR of the impulse response of each filter can be defined as the ratio of the area under the sidelobes to the area under the mainlobe, where those regions are defined to be the points below and above the -3 dB peak of the filter output

respectively. That ratio is

$$\mathrm{ISLR}_{\mathrm{IR}} \;=\; 20\log\left(\frac{\sum_{i:20\log\frac{|\bar{\mathbf{z}}(i)|}{\max(|\bar{\mathbf{z}}|)}<-3}\left|\bar{\mathbf{z}}(i)\right|}{\sum_{i:20\log\frac{|\bar{\mathbf{z}}(i)|}{\max(|\bar{\mathbf{z}}|)}\geq-3}\left|\bar{\mathbf{z}}(i)\right|}\right), \tag{21}$$

where $\bar{\mathbf{z}}(i)$ denotes the ith sample of the upsampled range profile. The ISLR is dependent on the range of delays considered and thus the scene size considered. Because of the relatively long symbol lengths of the OFDM signal used, the relevant scene size is likely to be smaller than the full range profile. Because of the frequency separation of the OFDM signal, the maximum scene size is approximately 10 km. If the image to be formed is significantly smaller than this, then the least-squares filter can be optimized within a particular scene size with a different weighting vector. In general, $\mathrm{ISLR}_{\mathrm{IR}}$ will consider the entire range profile except when a different range extent is specifically stated.

Range profiles for scenes consisting of multiple scatterers will also be used in this work. The primary purpose for these plots is to highlight the ability to identify smaller targets in a scene with a given filter. An example of a range profile with multiple scatterers is shown in Figure 3. In this work, range profiles depicted correspond to the pulse in the center of the receiver's flight path.

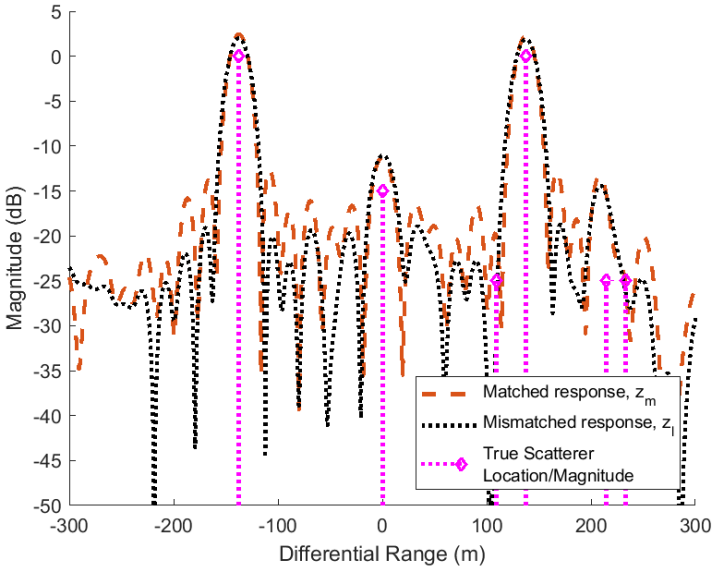

Figure 3: An example range profile of a matched and mismatched filter for a scene with multiple scatterers.

From Figure 3, several peaks along the range axis are evident from various scatterers. Because scatterers can have various reflectivities and can occur within the sidelobes of other scatterers, the ISLR metric is less useful for these examples since defining sidelobe and mainlobe areas is not possible. Instead they will serve primarily as a qualitative evaluation of performance.

2.9 PSF and SAR Images

The point spread function (PSF) is the 2-dimensional analog to the impulse response seen in the previous section. For a scene consisting of a single point scatterer at scene center, the PSF is created by using backprojection to combine the returns from each pulse along the aperture. Similar to the previous section, the PSF will be used as a tool to objectify performance by evaluating the ISLR. Note that while a mismatch loss metric could be done on the PSFs, this quantity is essentially the same as the average mismatch loss across the stack of range profiles and adds no further

insight.

Because sidelobe location and magnitude varies pulse to pulse, an ISLR calculation on the PSF however is not simply an average of the range profile ISLRs. For each PSF, an ISLR calculation will be done similar to the previous section using

$$\mathrm{ISLR}_{\mathrm{PSF}} \;=\; 20\log\left(\frac{\sum_{(x,y):20\log\frac{|\mathrm{PSF}(x,y)|}{\max(|\mathrm{PSF}|)}<-3}|\mathrm{PSF}(x,y)|}{\sum_{(x,y):20\log\frac{|\mathrm{PSF}(x,y)|}{\max(|\mathrm{PSF}|)}\geq-3}|\mathrm{PSF}(x,y)|}\right). \tag{22}$$

Whereas the range profile only shows the response of a single pulse with random additive noise, the PSF consists of many pulses each with their own independent noise. Because of this, perturbations that may be evident in the range profile for a given realization of noise will tend to average out in the PSF, providing a more consistent representation of the filter's performance. An example of a bi-static PSF is shown in Figure 4. Each image used in this work also shows the location of any relevant scatterers in the scene, depicted with magenta diamonds.

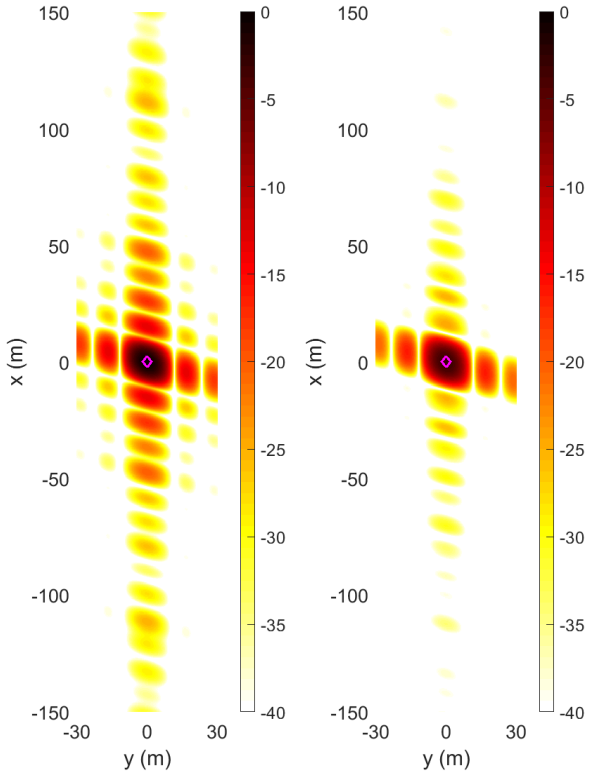

Figure 4: An example bi-static PSF of a matched (left) and mismatched (right) filter.

Note that because the PSF is computed by taking the ratio of image pixel intensities, the value of the ISLR_{PSF} for a given scenario depends on the image size. This work will use an image size of 300 m $\times$ 60 m throughout Chapter IV so that the same extent of sidelobes is considered for each example.

III. Mismatched Filter Formulation

3.1 Chapter Overview

This chapter introduces shortcomings of the traditional LSMMF and introduces a modified LSMMF (MLSMMF) to overcome these issues. The chapter begins with the traditional LSMMF's inability to allow for oversampled signals and proposes a new definition of the ideal response to resolve this. The bulk of the chapter focuses on how to rework the form of the mismatched filter in (19) to compensate for noise in the radar return signal. Examples are provided to show these changes in action to prepare the reader for a more thorough evaluation of the MLSMMF in Chapter IV. Portions of this Chapter were also published by the author in conference proceedings [15].

3.2 Modifications to the Least-Squares Definition

This section is used to expand the versatility of the LSMMF in (19). The definition will be generalized to allow for different sampling rates as well as providing a means to compensate for additive noise.

3.2.1 Ideal Response Definition

Previously, literature [1–4,6,7] has assumed the ideal response, $\mathbf{z}_i$ to be zero for all values outside the zero delay sample. This approach works when each sample of the signal is uncorrelated with nearby samples so that the mainlobe is a single impulse at the target range bin. This is unlikely to be the case in general though, because signals are typically sampled at a rate higher than the Nyquist rate and have some redundancy between samples.

For the case of oversampled signals, the redundant information caused by the oversampling will cause mainlobe spreading in the response. Application of the tra-

ditional least-squares approach of an impulse-like ideal response to an oversampled signal always results in very high mismatch loss. This loss is due to the fact that minimizing the zero delay response is less costly than having large values for the other off-peak mainlobe delays. This effect worsens as the oversampling factor increases. An example range profile formed from a LSMMF using an oversampled ($K = 2$) orthogonal frequency-division multiplexing (OFDM) signal and the impulse-like ideal response described above is shown in Figure 5. As expected, a very large mismatch loss of approximately 10 dB is observed.

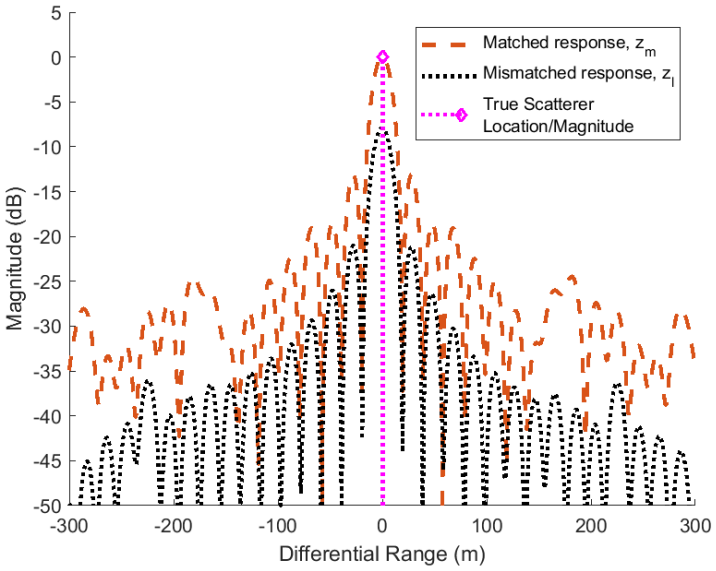

Figure 5: LSMMF response of an OFDM signal at twice the Nyquist sampling rate formed using an impulse-like ideal response, showing considerable mismatch loss.

To compensate for this factor in oversampled signals, the ideal response is modified in this work to have a spread mainlobe. For an oversampling factor of K, the mainlobe is considered to be the center $2\hat{K} - 1$ samples of the response where $\hat{K}$ is the integer nearest to K. These center $2\hat{K} - 1$ values of $\mathbf{z}_i$ are assumed to have values equal to the center $2\hat{K} - 1$ values of the matched filter response, $\mathbf{z}_m$, with all other values of

$\mathbf{z}_i$ being zero, that is

$$\mathbf{z}_i(k) = \begin{cases} \mathbf{z}_m(k), & -\hat{K}+1 < k < \hat{K}-1 \\ 0, & else \end{cases} \tag{23}$$

With this definition, the ideal response is assumed to have the same null-to-null mainlobe as the matched filter, with zero magnitude for all sidelobe values. Note that this modified definition of $\mathbf{z}_i$ is not necessarily the optimal definition, but produces adequate results for oversampled signals. The modified ideal response, $\mathbf{z}_i$, is shown along side the traditional impulse used for the ideal response in Figure 6.

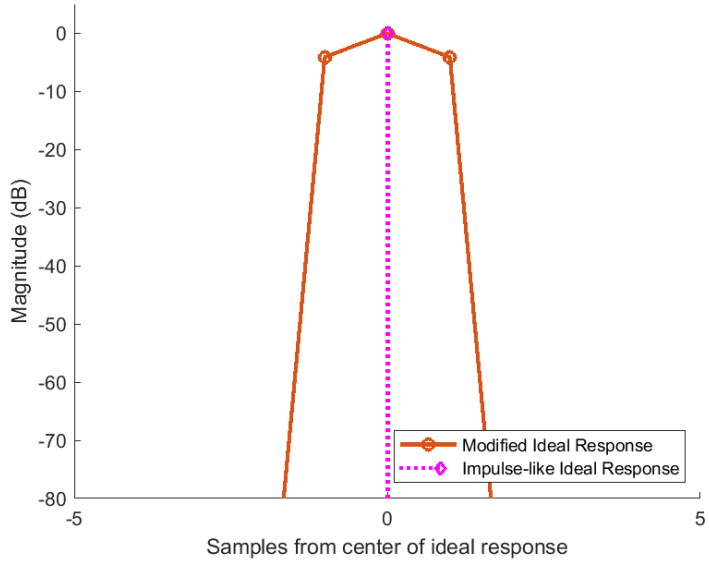

Figure 6: A depiction of the ideal response, $\mathbf{z}_i$ in (19), as both the traditional impulse and the modified spread response for a signal oversampled by a factor of $K = 2$.

The same example used in Figure 5 is repeated in Figure 7 using the new definition for the ideal response with all other variables identical. As expected, the new definition creates a response with only a small amount of mismatch loss, making it a viable definition for use when oversampling is used. The effect of sampling rate on SAR performance and why oversampling is a critical requirement is further explored

in Chapter IV.

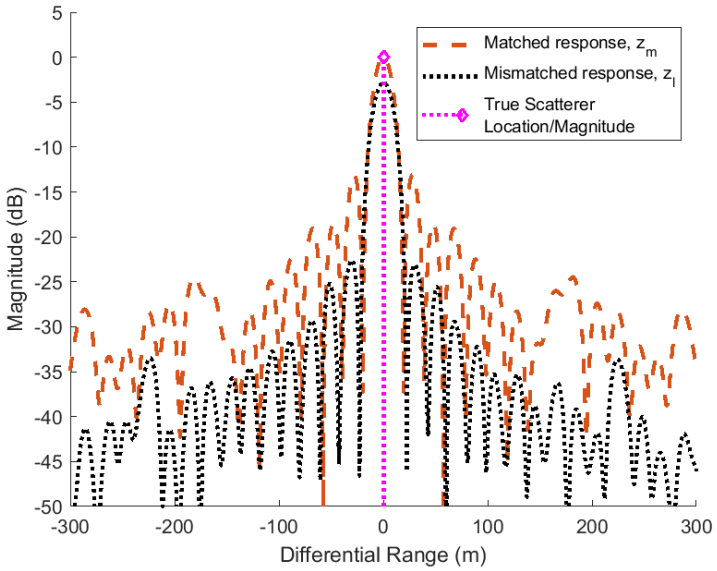

Figure 7: LSMMF response of an OFDM signal at twice the Nyquist sampling rate formed using the ideal response in (23).

3.3 Noise Compensation

With the ideal mainlobe now formulated, one remaining issue is that high filter coefficient values often occur in the LSMMF. These large coefficient values make the filter particularly susceptible to additive noise. To demonstrate, an OFDM signal oversampled by a factor of 2 with a moderate SNR of 0 dB is used as an example. The range profile formed from both the matched and LSMMF are shown in Figure 8.

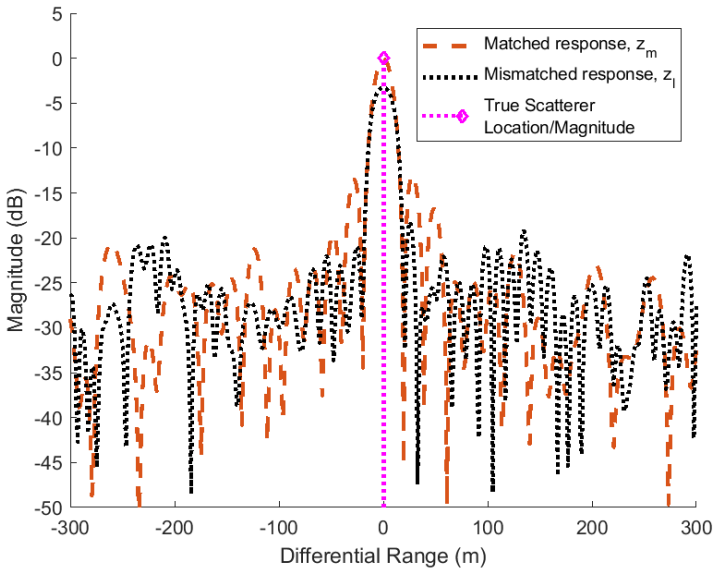

Figure 8: Range profiles for the matched filter and traditional LSMMF for a single point target and an SNR of 0 dB with the OFDM parameters specified in Chapter II.

From Figure 8, it is clear that no performance gain is realized from the LSMMF in the presence of noise. The filter still experiences noticeable mismatch loss and fails to reduce sidelobes in nearly all range bins. In this instance, the ISLR_{IR}(LSMMF) is 7.3 dB higher than the ISLR_{IR}(MF). In this noise regime, the LSMMF has no utility compared to the matched filter. To remedy this, the general form in (19) needs to be modified to compensate for noise effects.

To incorporate noise compensation into the filter design, the transmitted signal will be assumed to be corrupted with noise as in (14). Because the specific realization of noise is unknowable in advance, the filter will need to be designed around the statistics of the noise. First, the received signal $\mathbf{s}$ is assumed to be corrupted with additive noise $\mathbf{n}$. The convolution matrix of the received signal is then $\boldsymbol{\Theta}_s + \boldsymbol{\Theta}_n$.

Substituting this fact into (19) yields

$$\mathbf{h}_l = ((\mathbf{\Theta}_s + \mathbf{\Theta}_n)^H \mathbf{W} (\mathbf{\Theta}_s + \mathbf{\Theta}_n))^{-1} (\mathbf{\Theta}_s + \mathbf{\Theta}_n)^H \mathbf{W} \mathbf{z}_i \tag{24}$$

$$\mathbf{h}_l = (\mathbf{\Theta}_s^H \mathbf{W} \mathbf{\Theta}_s + \mathbf{\Theta}_s^H \mathbf{W} \mathbf{\Theta}_n + \mathbf{\Theta}_n^H \mathbf{W} \mathbf{\Theta}_s + \mathbf{\Theta}_n^H \mathbf{W} \mathbf{\Theta}_n)^{-1} (\mathbf{\Theta}_s + \mathbf{\Theta}_n)^H \mathbf{W} \mathbf{z}_i \tag{25}$$

$$\begin{aligned} \mathbf{h}_l = {} & (\mathbf{\Theta}_s^H \mathbf{W} \mathbf{\Theta}_s + \mathbf{\Theta}_s^H \mathbf{W} \mathbf{\Theta}_n + \mathbf{\Theta}_n^H \mathbf{W} \mathbf{\Theta}_s + \mathbf{\Theta}_n^H \mathbf{W} \mathbf{\Theta}_n)^{-1} \mathbf{\Theta}_s^H \mathbf{W} \mathbf{z}_i \\ & + (\mathbf{\Theta}_s^H \mathbf{W} \mathbf{\Theta}_s + \mathbf{\Theta}_s^H \mathbf{W} \mathbf{\Theta}_n + \mathbf{\Theta}_n^H \mathbf{W} \mathbf{\Theta}_s + \mathbf{\Theta}_n^H \mathbf{W} \mathbf{\Theta}_n)^{-1} \mathbf{\Theta}_n^H \mathbf{W} \mathbf{z}_i. \end{aligned} \tag{26}$$

Note that the entries of the terms $\mathbf{\Theta}_s^H \mathbf{W} \mathbf{\Theta}_n$ and $\mathbf{\Theta}_n^H \mathbf{W} \mathbf{\Theta}_s$ correspond to portions of the correlation of the signal $\mathbf{s}$ and the noise $\mathbf{n}$ which are independent. Because of this, the magnitudes of the entries in the resulting matrices are approximately zero and can be ignored in the mismatched filter formulation, resulting in

$$\mathbf{h}_l = (\mathbf{\Theta}_s^H \mathbf{W} \mathbf{\Theta}_s + \mathbf{\Theta}_n^H \mathbf{W} \mathbf{\Theta}_n)^{-1} \mathbf{\Theta}_s^H \mathbf{W} \mathbf{z}_i + (\mathbf{\Theta}_s^H \mathbf{W} \mathbf{\Theta}_s + \mathbf{\Theta}_n^H \mathbf{W} \mathbf{\Theta}_n)^{-1} \mathbf{\Theta}_n^H \mathbf{W} \mathbf{z}_i. \tag{27}$$

Similarly, the second term contains the product $\mathbf{\Theta}_n \mathbf{W} \mathbf{z}_i$ which corresponds to a portion of the correlation between the noise $\mathbf{n}$ and the ideal response $\mathbf{z}_i$ which are independent. Again, this forces the magnitude of the entries in the second term to be approximately zero resulting in

$$\mathbf{h}_l = (\mathbf{\Theta}_s^H \mathbf{W} \mathbf{\Theta}_s + \mathbf{\Theta}_n^H \mathbf{W} \mathbf{\Theta}_n)^{-1} \mathbf{\Theta}_s^H \mathbf{W} \mathbf{z}_i. \tag{28}$$

The term $\mathbf{\Theta}_n^H \mathbf{W} \mathbf{\Theta}_n$ relates to the convolution of noise with itself and forms approximately a diagonal matrix. The expectation of this term is designated as the noise compensation term, $\mathbf{A}$. In the case of uniform weighting, $\mathbf{A}$ is approximately

$$\mathbf{A} = E\left[\mathbf{\Theta}_n^H \mathbf{W} \mathbf{\Theta}_n\right] \approx P_n N K \mathbf{I}, \tag{29}$$

where NK is the signal length, P_n is the average noise power, and $\mathbf{I}$ is the identity matrix. Note that $\mathbf{A}$ is a diagonal matrix that is $NK \times NK$.

For a general weighting vector, the noise compensation term is still a diagonal matrix and the ith term along the diagonal is approximately

$$\mathbf{A}(i,i) \approx P_n \sum_{k=i}^{NK+i-1} W(k). \tag{30}$$

At this point, the mismatched filter coefficients depends only on the signal itself and the average power of the noise

$$\mathbf{h}_l = (\mathbf{\Theta}_s^H \mathbf{W} \mathbf{\Theta}_s + \mathbf{A})^{-1} \mathbf{\Theta}_s^H \mathbf{W} \mathbf{z}_i. \tag{31}$$

In the presence of noise and with non-uniform weighting vectors, the magnitude of $\mathbf{A}$ can have a significant effect on the magnitude of the filter coefficients. To allow for comparison between this newly formed MLSMMF and the matched filter, a scale factor α is included when noise is present so that

$$\mathbf{h}_l = \alpha(\mathbf{\Theta}_s^H \mathbf{W} \mathbf{\Theta}_s + \mathbf{A})^{-1} \mathbf{\Theta}_s^H \mathbf{W} \mathbf{z}_i. \tag{32}$$

In the presence of noise, the scale factor α is set such that $|\mathbf{h}_l|^2 = |\mathbf{h}_m|^2$. In the case of zero noise, α is defined to be equal to 1 and (32) reduces to (19). Note that the scale factor has no effect on the ISLR whose improvement is due to the diagonal loading term. To show the effect of the MLSMMF defined in (32), the example from the beginning of the section will be revisited. Again, the exact same OFDM signal oversampled by a factor of 2 with a moderate SNR of 0 dB is used. The range profile formed from both the matched filter and MLSMMF are shown in Figure 9.

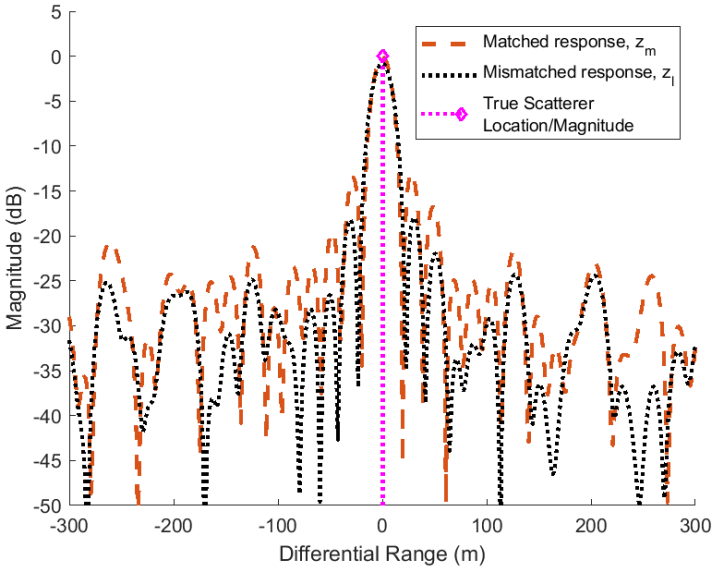

Figure 9: Range profiles for the matched filter and MLSMMF for a single point target and an SNR of 0 dB with the OFDM parameters specified in Chapter II.

In this case, the effect of mismatch loss is not apparent because of the scale factor α being used for comparison, however sidelobe suppression is noticeably better with an ISLR_{IR}(MLSMMF) that is 1.4 dB lower than the ISLR_{IR}(MF). Recall that previously without noise compensation, the ISLR of the LSMMF was significantly worse than the matched filter. The addition of a simple noise compensation term, $\mathbf{A}$, dependent only on the average noise power has significantly increased filter performance.

The addition of a diagonal loading term has appeared in other works such as [16] as a means of compensating for the ill-conditioning of $\boldsymbol{\Theta}_s^H \boldsymbol{\Theta}_s$ when the signal is oversampled, where it is shown that the magnitude of the loading factor influences the tradeoff between sidelobe suppression and mismatch loss. In this paper however, (32) specifies the optimal loading factor to be used for a given SNR to minimize the sidelobes. The sensitivity of the noise compensation term $\mathbf{A}$ to changes in magnitude and structure in relation to performance of the MLSMMF will be explored further in Chapter IV.

IV. Results and Analysis

4.1 Chapter Overview

This chapter explores the concepts introduced in Chapter III and shows the results of varying parameters in the MLSMMF. First, the effects of oversampling will be shown at various oversampling rates. Next, the performance of the MLSMMF will be compared to that of the matched filter in various noise environments for a single point target. Variations to the weight vector will be used to show how given some a priori knowledge of the scene, the MLSMMF's performance can be further improved even in the presence of high noise levels. Scenes consisting of multiple scatterers will then be used to illustrate how small scatterers can be hard to identify when sidelobes have little suppression as with the matched filter. Clutter will be used as an additional multiple scatterer scene to illustrate how the addition of clutter to noise further degrades image quality. Next, the noise compensation term of the MLSMMF will be compared to similar compensation terms. Finally, the chapter will conclude with a comparison to phase history windowing as an additional technique to reduce sidelobes.

4.2 Oversampling Effects

As alluded to in Chapter III, oversampling of signals is used in this work. The reason for this is that in practice, radar targets can exist at any range in the continuous landscape; however, with the digital process employed, the filter response can only be minimized at discrete range bins. When a critically sampled signal is used, these discrete range bins in the filter response happen to occur at the peak of the filter response, as well as at each null in the response. With this perspective, the traditional ideal filter response introduced in Chapter III consisting of an impulse is the logical

choice as it would optimize the filter performance at those particular range bins. The performance at ranges between those range bins is unaccounted for however. Furthermore, because the sample points of the critically sampled response occur at nulls in the response, the filter response appears to have exceptional performance. Unfortunately, when the response is interpolated to a finer grid, as is typically done in backprojection imaging, much of this apparent performance disappears.

An example of a mismatch filter response for a critically sampled signal with no additive noise and the same response interpolated to a grid that is 128 times finer is shown in Figure 10a. Note that the critically sampled response tracks closely to the nulls of the response that is interpolated to a finer grid. That is to say that the two plots roughly agree with each other at the sample points, but the interpolated plot gives a visual representation that is more faithful to what the true continuous response would be. Similarly, metrics such as the ISLR of the interpolated response are more faithful to true performance in the continuous physical landscape.

Because backprojection uses interpolation to accumulate the contribution of each pulse onto an image grid, it is desirable that the performance of the individual mismatched filters be a good indicator of the quality of the produced range profiles used to create the image. By using a higher sampling rate, the mismatch filter will also appear closer to what the true continuous range profile would be and when interpolated to create an image grid, will show better performance. To illustrate this, oversampling ratios ranging from 2 to 8 are used. Figure 10b shows the filter response of a signal oversampled by a factor of 2 and the same response interpolated to a grid at 128 times the Nyquist rate. Figure 11a and Figure 11b are similar plots showing oversampling rates of $K = 4$ and $K = 8$ respectively. Note that as the oversampling rate increases, the filter response much more closely agrees with the interpolated response which is used to form the image.

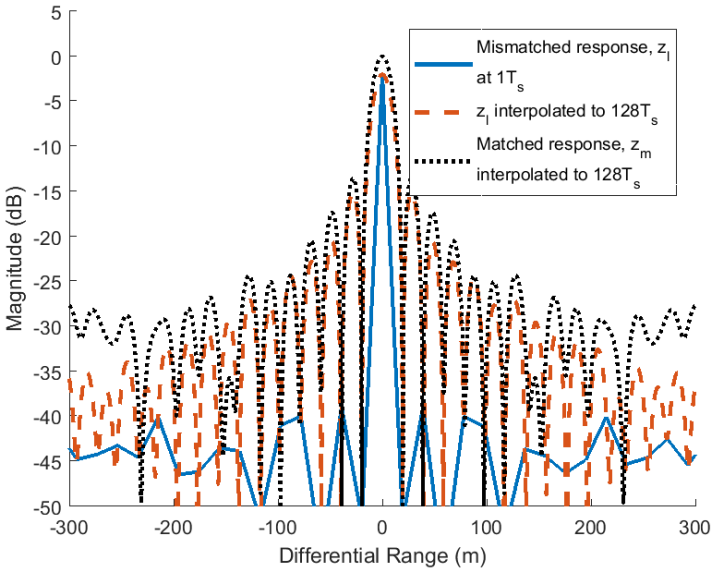

(a) Sampled at K = 1

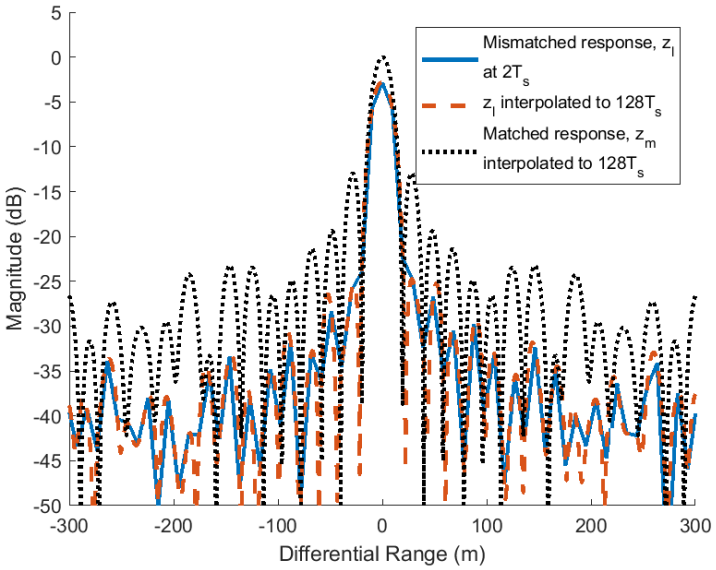

(b) Sampled at K = 2

Figure 10: MLSMMF response of an OFDM signal at the given sampling rate and the same response interpolated to a grid that is 128 times finer than the Nyquist sampling.

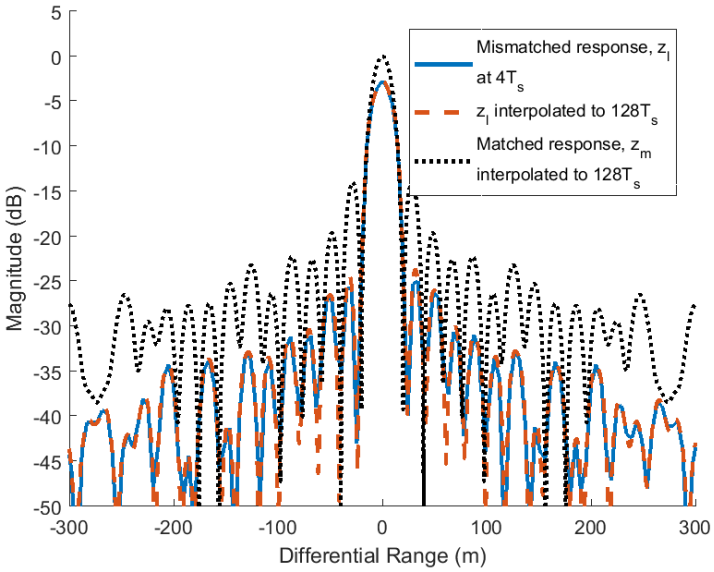

(a) Sampled at K = 4

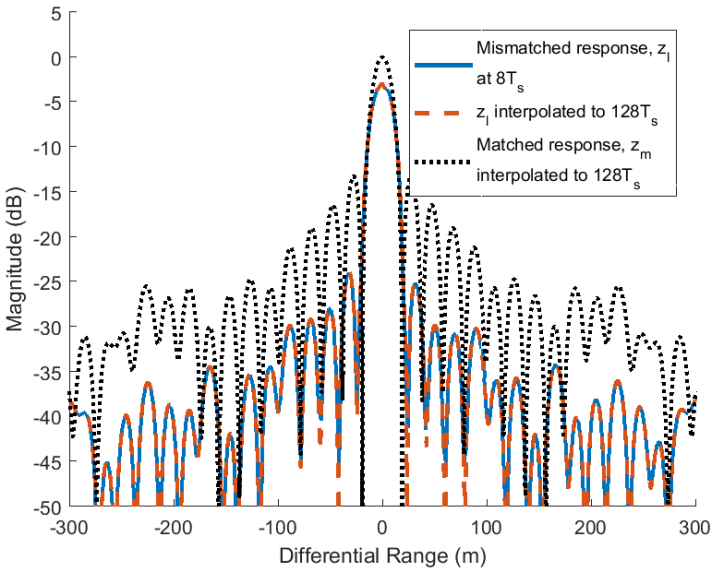

(b) Sampled at K = 8

Figure 11: MLSMMF response of an OFDM signal at the given sampling rate and the same response interpolated to a grid that is 128 times finer than the Nyquist sampling.

The ISLR, range resolution, and mismatch loss of the interpolated range profiles averaged over 41 signals are tabulated in Table 2. Note that the ISLR of the MLSMMF generally improves with increased oversampling since the least-squares

process has more tunable coefficients to achieve the ideal response, although these improvements decrease as the oversampling rate increases. The oversampling rates of 2, 4, and 8 perform particularly well since these rates have sample points coinciding with the maxima of the response which are the most relevant points to reduce via least-squares. The matched filter shows no improved performance with increased sampling rate as expected.

Note that because of the definition of the ideal response in (23), the $K = 1.25$ case is just a traditional LSMMF with no mainlobe spreading in the ideal response. Even with the small amount of oversampling, the mismatch loss is noticeably higher for this case with $L = 3.87$ dB.

When mainlobe spreading in the ideal response definition is implemented as with all values of $K \geq 1.5$, the mismatch loss is relatively constant around 2.85 dB. This ideal response definition however does result in a significant spreading in the mainlobe. From (2), the approximate Rayleigh resolution is approximately 10.10 m; however, the measured range resolutions will be smaller since they are measured using the mainlobe -3dB width definition in Chapter II [9]. The measured range resolution for the matched filter was 9.30 m and did not change with oversampling rate. The measured range resolution for the MLSMMF varied with oversampling rate due to the modified definition of $\mathbf{z}_i$ in (23), but was always worse than the matched filter resolution when $K \geq 1.5$. The degradation in resolution was the lowest at 13.5 percent for $K = 2$ and the highest at 22 percent for $K = 4$.

A coarser resolution is not the only drawback to consider with the MLSMMF. The higher sampling rates lead to multiple other considerations. One of these is monetary cost due to the increased hardware requirements associated with sampling at higher rates and storing more data. Another considerable factor is processing time. Because the LSMMF uses multiple matrix multiplications and an inverse operation,

it in general runs in $O(NK)^3$ time. There are specialized algorithms that can reduce this time; however, a significant increase in oversampling rate will nonetheless cause a dramatic increase in processing time. Because of this time versus performance tradeoff, an oversampling factor of $K = 2$ is used throughout the remainder of this work.

Table 2: Average ISLR_{IR}, measured PSF range resolution, and mismatch loss, L, at various levels of oversampling

K	ISLR_{IR}(MF)	ISLR_{IR}(MLSMMF)	ρ_u(MF)	ρ_u(MLSMMF)	L
1	27.60	22.42	9.30	9.30	2.0050
1.25	27.59	22.37	9.30	9.30	3.87
1.5	27.57	20.65	9.30	10.87	2.94
1.75	27.59	20.76	9.30	10.72	2.82
2	27.63	20.90	9.30	10.56	2.85
3	27.63	20.65	9.30	11.03	2.87
4	27.61	20.35	9.30	11.35	2.84
5	27.61	20.41	9.30	11.19	2.87
6	27.63	20.48	9.30	11.12	2.87
7	27.61	20.47	9.30	11.19	2.86
8	27.62	20.34	9.30	11.19	2.85

4.3 MLSMMF in Noise for a Single Point Target

In this section, the MLSMMF will be compared to the matched filter across a number of varying SNRs. The SNRs to be used will be ∞, 10 dB, 0 dB, and -10 dB. The 10 dB case is used to represent a case with low noise, where the received signal is dominated by the desired signal. The 0 dB case acts as a moderate noise case where the received signal magnitude is similar to the noise magnitude in the relevant frequency band. The -10 dB case is used to represent a high noise case where the received signal is dominated with noise unrelated to the desired signal. In this work, the SNR is defined as

$$\text{SNR (dB)} \;=\; 10\log_{10}\frac{\sum_i |\mathbf{s}(i)|^2}{\sum_i |\mathbf{n}(i)|^2}, \tag{33}$$

where $\mathbf{s}(i)$ is the ith sample of the transmitted signal and $\mathbf{n}(i)$ is the ith sample of the additive noise.

4.3.1 No Noise, SNR = ∞

In this example, a noiseless environment is considered. A typical response formed from both a matched filter and the MLSMMF for the same signal is shown in Figure 12a. From the figure it is clear that the mismatched response has significantly reduced sidelobes while only exhibiting a small amount of mismatch loss in the mainlobe. Averaged over 41 different waveforms, the ISLR_{IR} of the MLSMMF is 20.86 dB while the ISLR_{IR} of the matched filter is 27.59 dB. The MLSMMF of sidelobes in this case is significant and is accompanied by a mismatch loss of 2.82 dB.

The image formed over the 2 degree aperture is shown in Figure 12b for the matched filter and in Figure 12c for the MLSMMF. The ISLR_{PSF} for the MLSMMF is 11.74 dB while the ISLR_{PSF} of the matched filter is 15.24 dB. The sidelobe reduction

seen in the PSF of the MLSMMF is significant along the range direction as expected with sidelobe magnitude falling below the 40 dB image threshold in approximately 100 m. There is no significant effect in the cross-range dimension as expected, as the filter used can only impact sidelobes along the range dimension.

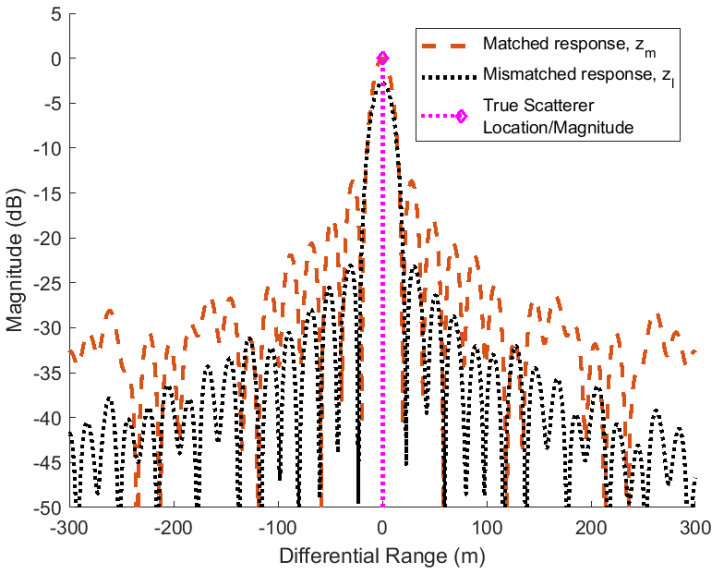

(a) Zoomed impulse response for center pulse

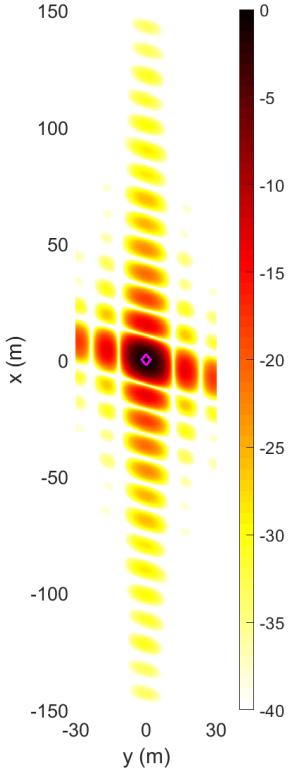

(b) PSF formed from Matched Filter

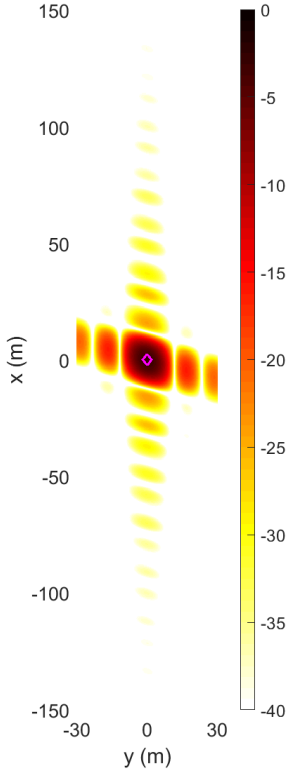

(c) PSF formed from MLSMMF

Figure 12: The impulse response (a) and PSFs formed using a matched filter (b) and MLSMMF (c) with uniform weighting for an SNR of ∞ using the OFDM signal parameters specified in Chapter II.

4.3.2 Low Noise, SNR = 10 dB

In this example, the same set of signals is used with a small amount of noise added to the received signals such that the SNR = 10 dB. A typical response formed from both a matched filter and the MLSMMF for the same signal is shown in Figure 13a. The MLSMMF result is very similar to that seen in Figure 12a, indicating that the small amount of noise has little effect on the matched filter and the MLSMMF.

The matched filter is inherently noise tolerant due to its structure. Convolving the received signal with the time reversed conjugate of the signal is essentially taking the autocorrelation of the signal. Because of this, additive noise in the return signal has little effect on the response, particularly when the magnitude of the noise is small. The addition of the noise compensation in the MLSMMF achieves the same effect unlike the traditional LSMMF. Averaged over 41 different waveforms, the ISLR_{IR} of the MLSMMF is 22.93 dB while the ISLR_{IR} of the matched filter is 27.94 dB. With additive noise, the ISLR_{IR} of the MLSMMF degrades more than that of the matched filter, but still represents a noticeable improvement. The average mismatch loss with additive noise is 1.64 dB.

The image formed over the 2 degree aperture is shown in Figure 13b for the matched filter and in Figure 13c for the MLSMMF. The ISLR_{PSF} for the MLSMMF is 12.33 dB while the ISLR_{PSF} of the matched filter is 15.30 dB. The sidelobe reduction seen in the PSF for the MLSMMF is significant along the range direction as expected when compared to the matched filter, similar to the previous example.

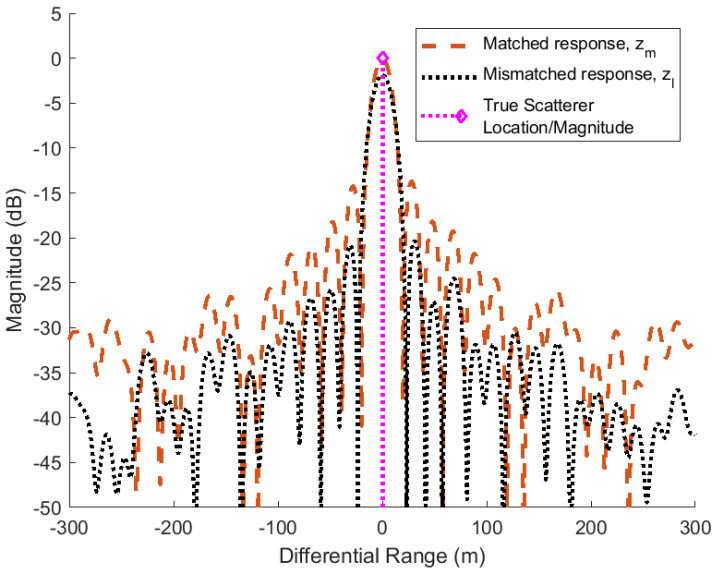

(a) Zoomed impulse response for center pulse

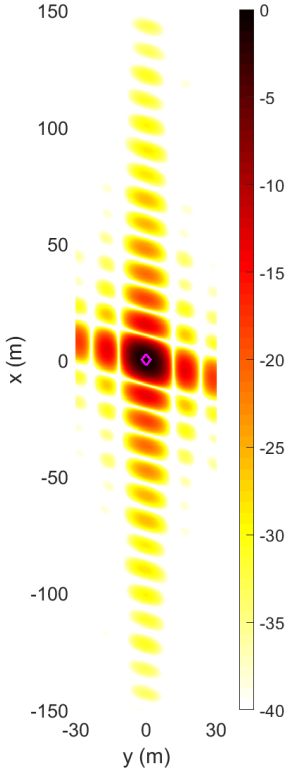

(b) PSF formed from Matched Filter

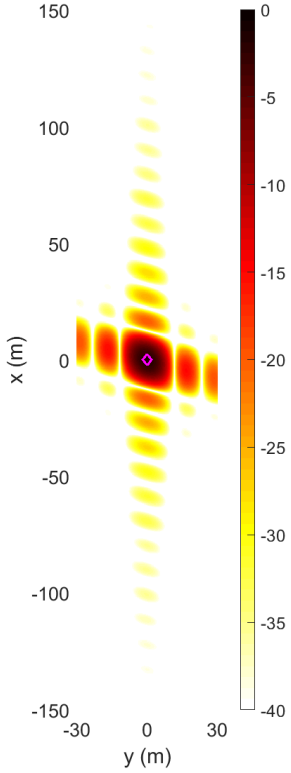

(c) PSF formed from MLSMMF

Figure 13: The impulse (a) and PSFs formed using a matched filter (b) and MLSMMF (c) with uniform weighting for an SNR of 10 dB using the OFDM signal parameters specified in Chapter II.

4.3.3 Moderate Noise, SNR = 0 dB

In this example, the same signals are again used for each pulse, and a moderate amount of noise is added to the received signals such that the SNR = 0 dB. A typical profile formed from both a matched filter and the MLSMMF for the same signal is shown in Figure 14a. This result is slightly degraded compared to that seen in the previous examples, indicating that the moderate amount of noise is beginning to have an effect on the matched filter and the MLSMMF. Averaged over 41 different waveforms, the ISLR_{IR} of the MLSMMF is 28.22 dB while the ISLR_{IR} of the matched filter is 30.24 dB. The average mismatch loss in this example is 0.74 dB. Note that while the mismatch loss appears to be decreasing with SNR, this is merely a result of using a logarithmic scale and the fact that the proportion of mainlobe energy caused by the desired signal is reducing.

The image formed over the 2 degree aperture is shown in Figure 14b for the matched filter and in Figure 14c for the MLSMMF. The ISLR_{PSF} for the MLSMMF is 12.92 dB while the ISLR_{PSF} of the matched filter is 15.57 dB. The sidelobe reduction seen in the PSF for the MLSMMF is significant along the range direction as expected when compared to the matched filter, similar to the previous example. At this SNR, the sidelobes of the MLSMMF continue to increase in magnitude and are evident in the PSF across the entire range extent of the image.

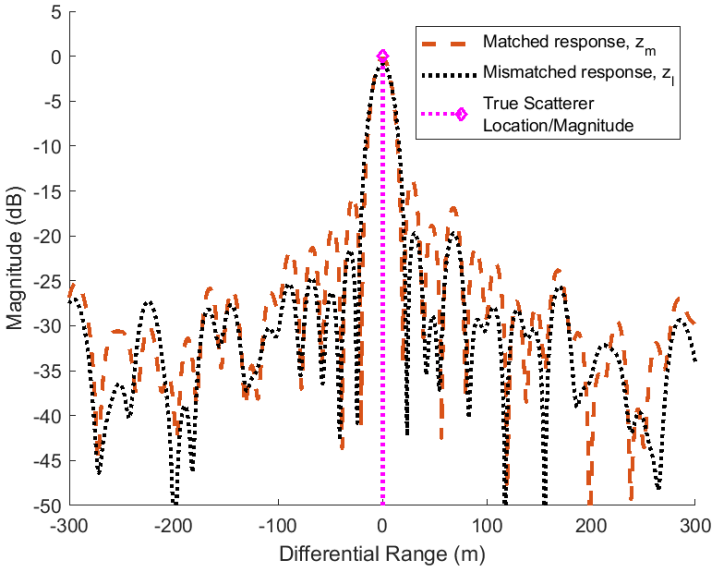

(a) Zoomed impulse response for center pulse

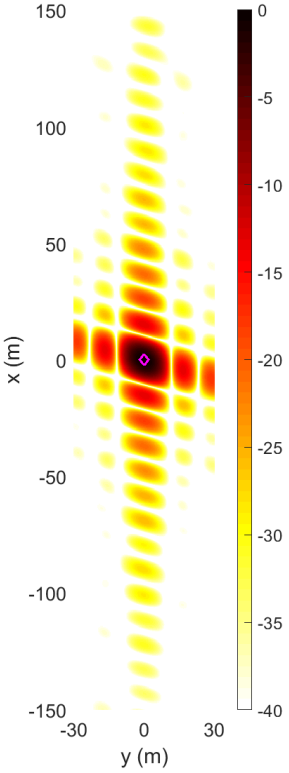

(b) PSF formed from Matched Filter

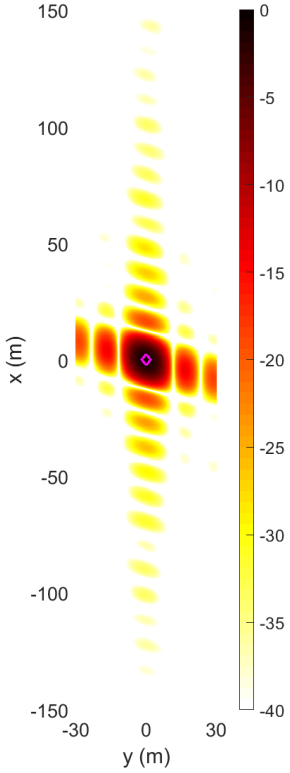

(c) PSF formed from MLSMMF

Figure 14: The impulse response (a) and PSFs formed using a matched filter (b) and MLSMMF (c) with uniform weighting for an SNR of 0 dB using the OFDM signal parameters specified in Chapter II.

4.3.4 High Noise, SNR = -10 dB

In this example, the same signals are again used for each pulse, and a large amount of noise is added to the received signals such that the SNR = -10 dB. A typical profile formed from both a matched filter and the MLSMMF for the same signal is shown in Figure 15a. This result is noticeably degraded compared to that seen in the previous examples with multiple sidelobes approaching a magnitude of -20 dB, indicating that the large amount of noise is having a significant effect on the matched filter and the MLSMMF. Averaged over 41 different waveforms, the ISLR_{IR} of the MLSMMF is 36.41 dB while the ISLR_{IR} of the matched filter is 37.24 dB. The average mismatch loss in this example is 0.25 dB. Even with the large amount of noise, the MLSMMF still shows a slight improvement over that of the matched filter.

The image formed over the 2 degree aperture is shown in Figure 15b for the matched filter and in Figure 15c for the MLSMMF. The ISLR_{PSF} for the MLSMMF is 14.91 dB while the ISLR_{PSF} of the matched filter is 16.93 dB. The sidelobe reduction seen in the PSF for the MLSMMF is significant along the range direction as expected when compared to the matched filter, similar to the previous example. At this SNR, the sidelobes of the MLSMMF have further increased and the PSF is also full of additional spots along both range and cross-range caused by the noise.

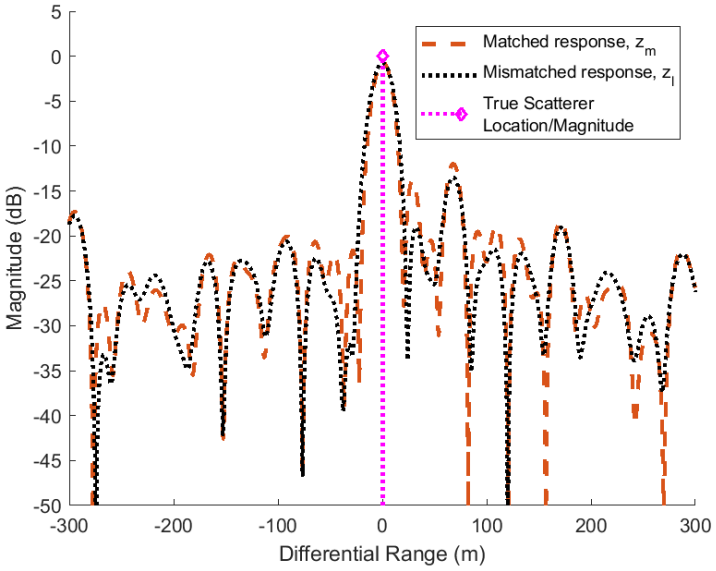

(a) Zoomed impulse response for center pulse

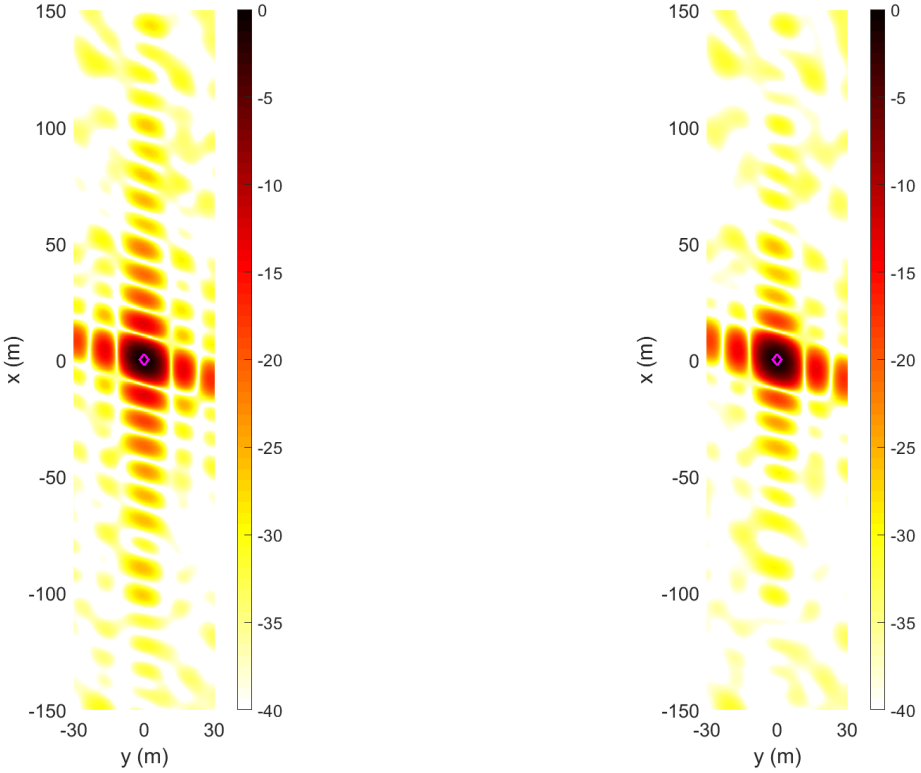

(b) PSF formed from Matched Filter

(c) PSF formed from MLSMMF

Figure 15: The impulse response (a) and PSFs formed using a matched filter (b) and MLSMMF (c) with uniform weighting for an SNR of −10 dB using the OFDM signal parameters specified in Chapter II.

4.3.5 Single Target Summary for Uniform Weighted MLSMMF

The results from the previous examples spanning multiple SNRs are summarized in Table 3. At each SNR, the MLSMMF showed superior sidelobe MLSMMF when compared to the matched filter. As the signal becomes more noise dominant, the performance improvement of the MLSMMF decreases however. This is particularly true for the change between a noiseless scene and a scene with an SNR of 10 dB where the ISLR of the matched filter decreased by less than 0.5 dB in the range profile and less than 0.1 dB in the PSF, whereas the MLSMMF saw degradations of approximately 2.1 dB and 0.6 dB respectively. That is to say, while the MLSMMF is tolerant to noise and still shows improvement over the matched filter at all SNRs, the performance increase is most significant when there is low noise.

Another key characteristic of the MLSMMF across all SNRs is that the width of the mainlobe increased by approximately 19 percent. Because range resolution is dependent on the mainlobe width, this means that a loss in range resolution is another drawback of the LSMMF. This is a drawback that may be reducible by modifying the ideal response definition in (23).

Table 3: Summary of ISLR and mismatch loss across various SNRs

SNR	ISLR_{IR}(MLSMMF)	ISLR_{IR}(MF)	ISLR_{PSF}(MLSMMF)	ISLR_{PSF}(MF)	L
∞	20.86	27.59	11.74	15.24	2.82
10	22.93	27.94	12.33	15.30	1.64
0	28.22	30.24	12.92	15.57	0.74
-10	36.41	37.24	14.91	16.93	0.25

4.4 MLSMMF in Noise for Varying Weighting Vectors

Prior to this section, the MLSMMFs that have been implemented have used a uniform weighting vector, that is, a weighting vector, $\mathbf{W}$, consisting of all 1's. This choice of vector means the least-squares cost function treats every range bin equally and will try to minimize the sidelobes across the entire scene. If significant scatterers in a scene are confined to a tight area however, sidelobes outside of a significantly smaller range may be irrelevant. This section will explore 2 different weighting vectors, each taking the form of a rectangular function. These weighting vectors will be shown to be able to further minimize sidelobes near the target at the expense of having larger sidelobes far away from the target.

4.4.1 No Noise, SNR = ∞, Wide Rectangular Weighting Vector

To begin with, a single point scatterer will be considered with no additive noise. The weighting vector, $\mathbf{W}$, in this example will consist of all 1's for the center 20 percent of values, with values of near zero for all other entries. In terms of the least-squares cost function, this will weight any deviation from the ideal response equally for the center 20 percent of range bins, but will carry a negligible cost for range bins outside of this region. Near zero values are used instead of zero values to prevent ill conditioned matrices in the least-squares computation. Figure 16a shows a typical response formed from this wide rectangular weighted MLSMMF compared against the corresponding matched filter response. A significant dropoff in sidelobe magnitude occurs, with the sidelobes being approximately 20 dB lower than those of the matched filter. When compared to the uniform example in Figure 12a, significant performance increase is also seen.

Outside of the inner 20 percent of the response however, sidelobes are considerably worse. To show this, the previous response is shown across the entire range profile

in Figure 16b. In the figure, it is clear that there is a sharp rise in the sidelobes where the weighting vector held near zero values. Because of this, the ISLR across the full range is 37.03 dB, significantly worse than both the uniform weighting vector case and the matched filter. If however, the ISLR is only computed over the inner 20 percent of the range profile, the ISLR of the response using the wide rectangular weighting vector is -0.96 dB, compared to 8.12 dB for the uniform weighted vector and 15.68 dB for the matched filter. That is, the performance difference by using the wide rectangular weighting vector over the uniform weighting vector is greater than the performance difference between the uniform MLSMMF and the matched filter.

The image formed over the 2 degree aperture is shown in Figure 17a for the matched filter and in Figure 17b for the MLSMMF. The ISLR_{PSF} for the MLSMMF is 9.22 dB while the ISLR_{PSF} of the matched filter is 15.24 dB. Recall from earlier, that the uniformly weighted MLSMMF produced an image with a ISLR_{PSF} of 11.74 dB. For the given single target scene and the image area used, this choice of weighting vector shows a noticeable improvement in sidelobe MLSMMF.

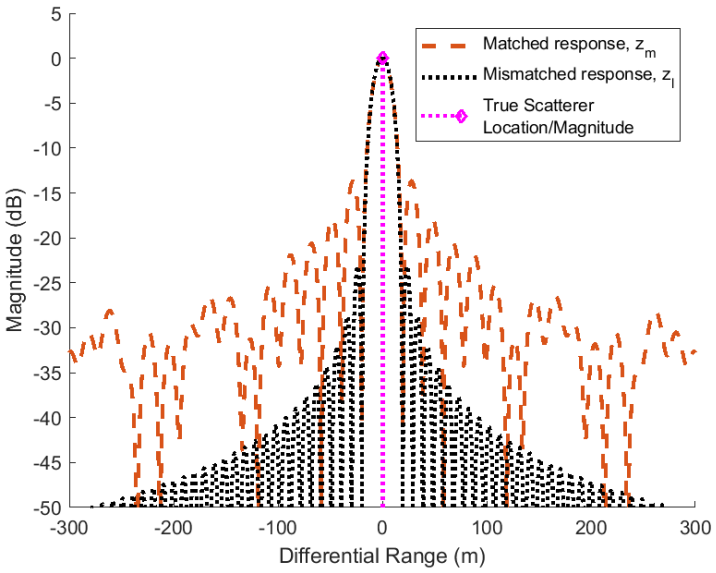

(a) Zoomed impulse response for center pulse

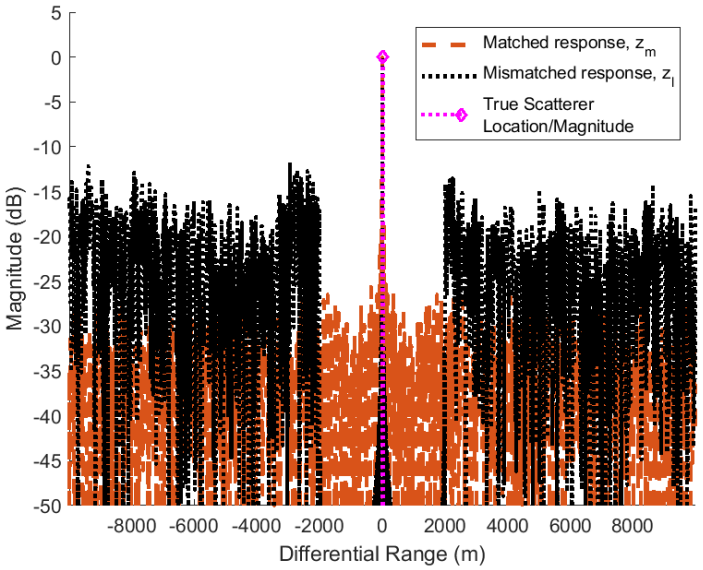

(b) Full impulse response for center pulse

Figure 16: The zoomed impulse response (a) and full impulse response for a matched filter and MLSMMF with wide rectangular weights for an SNR of ∞ using the OFDM signal parameters specified in Chapter II.

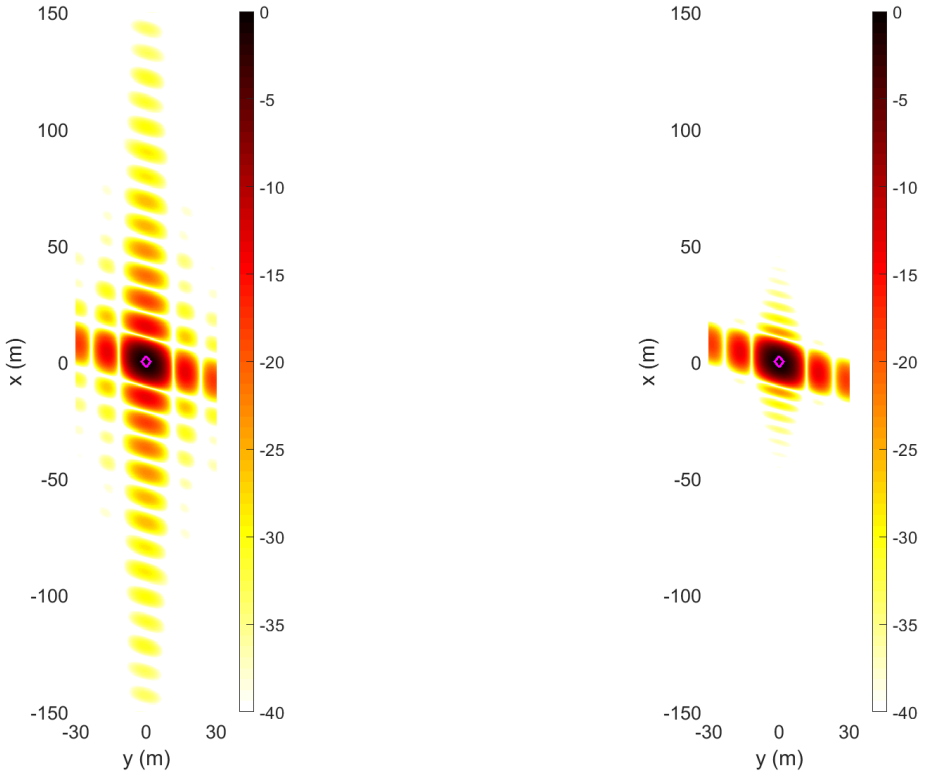

(a) PSF formed from Matched Filter

(b) PSF formed from MLSMMF

Figure 17: PSFs formed using a matched filter (a) and MLSMMF (b) with wide rectangular weights for an SNR of ∞ using the OFDM signal parameters specified in Chapter II.

4.4.2 Moderate Noise, SNR = 0 dB, Wide Rectangular Weighting Vector

This example extends the MLSMMF described in the previous example to a scene consisting of moderate noise. Figure 18a shows a typical zoomed in response formed from this wide rectangular weighted MLSMMF compared against the corresponding matched filter response for an SNR of 0 dB. The full response is shown in Figure 18b. The effect of the additive noise disrupts much of the performance increase of the MLSMMF, similar to the uniform weighting case. The ISLR computed over the inner 20 percent of the range profile for this wide rectangular weighting vector is 14.79 dB, compared to 15.67 dB for the uniform weighted vector and 18.08 dB for the matched

filter. In this case, the use of the wide rectangular weighting vector shows much less improvement now that noise is a significant factor.

The image formed over the 2 degree aperture is shown in Figure 19a for the matched filter and in Figure 19b for the MLSMMF. The ISLR_{PSF} for the MLSMMF is 12.78 dB while the ISLR_{PSF} of the matched filter is 15.57 dB. Recall from earlier, that the uniformly weighted MLSMMF produced an image with a ISLR_{PSF} of 12.92 dB. Again, the performance increase by using the different weighting vector is significantly reduced with the addition of noise. The addition of the noise compensation term in (32) does still allow the weighted filter to perform better than the matched filter over the area of interest however.

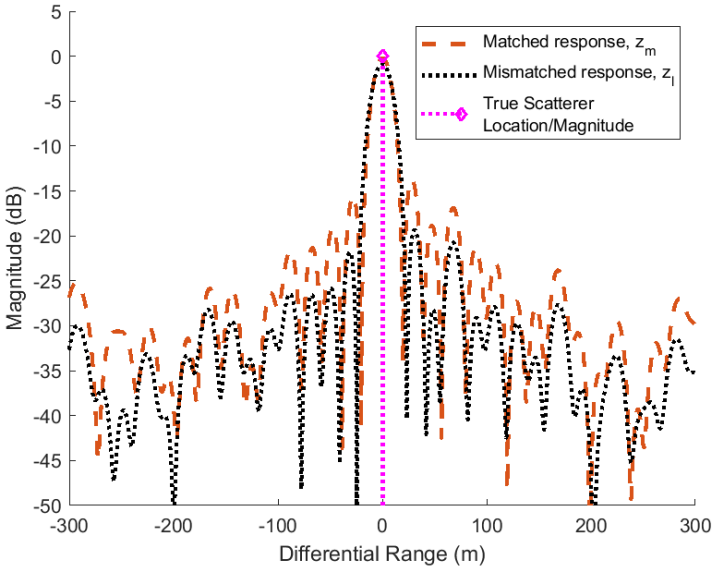

(a) Zoomed impulse response for center pulse

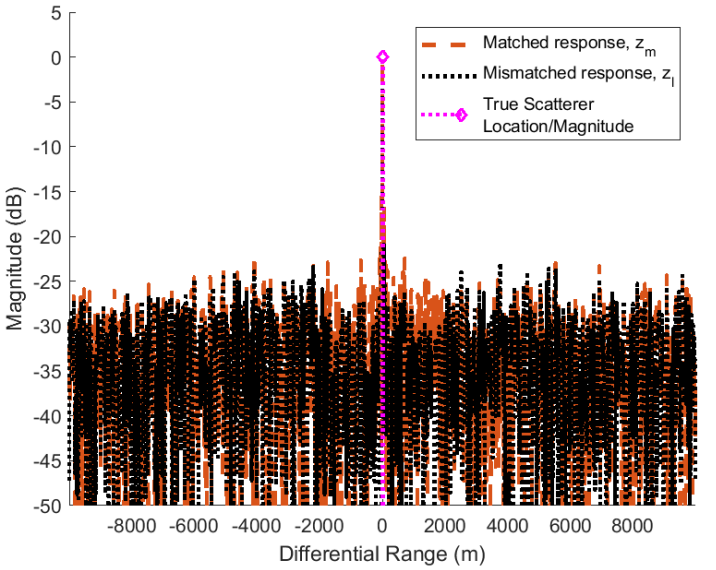

(b) Full impulse response for center pulse

Figure 18: The zoomed impulse response (a) and full impulse response for a matched filter and MLSMMF with wide rectangular weights for an SNR of 0 dB using the OFDM signal parameters specified in Chapter II.

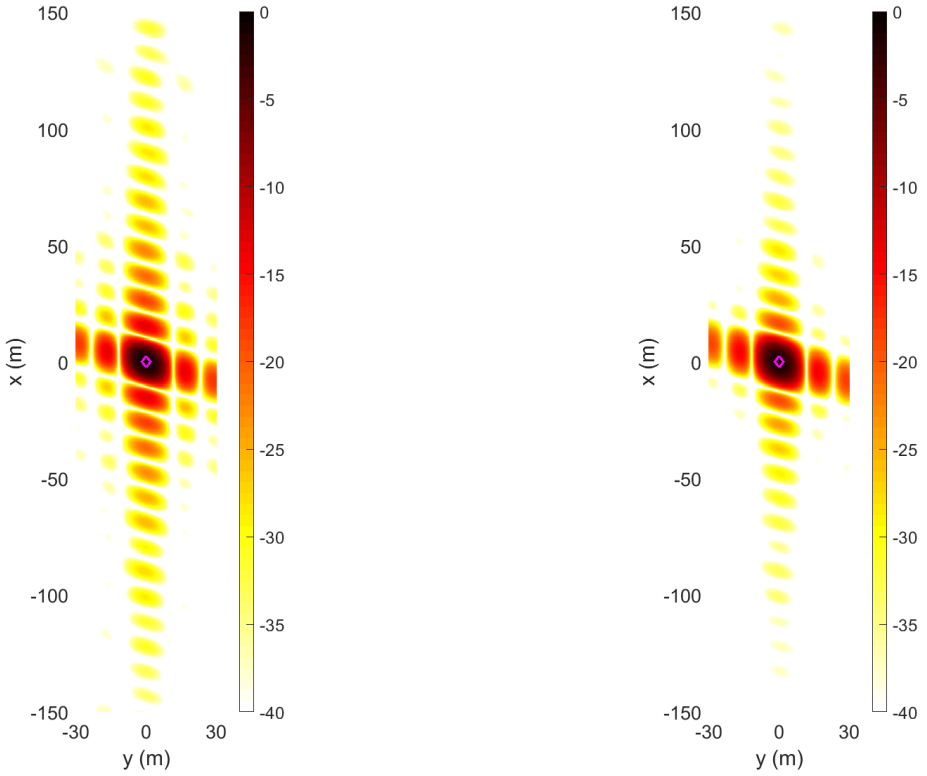

(a) PSF formed from Matched Filter

(b) PSF formed from MLSMMF

Figure 19: PSFs formed using a matched filter (a) and MLSMMF (b) with wide rectangular weights for an SNR of 0 dB using the OFDM signal parameters specified in Chapter II.

4.4.3 No Noise, SNR = ∞, Narrow Rectangular Weighting Vector

By further reducing the size of the rectangular weighting vector, improvement can be further increased over an even smaller range interval. The weighting vector, $\mathbf{W}$, in this example will consist of all 1's for the center 2 percent of values, with values of near zero for all other entries. Figure 20a shows a typical zoomed in response formed from this narrow rectangular weighted MLSMMF compared against the corresponding matched filter response for an noiseless signal. The full response is shown in Figure 20b. As expected, the sidelobes are suppressed exceptionally well over a narrow area before increasing to levels significantly higher than the those of the matched filter. The ISLR computed over the inner 2 percent of the range profile for this narrow rectangular

weighting vector is -2.67 dB, compared to 15.67 dB for the uniform weighted vector and 4.86 dB for the matched filter.

The image formed over the 2 degree aperture is shown in Figure 21a for the matched filter and in Figure 21b for the MLSMMF. The ISLR_{PSF} for the MLSMMF is 16.15 dB while the ISLR_{PSF} of the matched filter is 15.24 dB. This decrease is because of the high sidelobes occurring approximately 100 meters up and down range from the target. These sidelobes represent a blur effect on the image, except rather than blurring nearby areas of the image, the blur affects more distant areas. Because of this significant blurring, the rectangular weighting vector only has utility when scatterers within the scene extent are confined to a small area corresponding to the width of the rectangular weighting vector used.

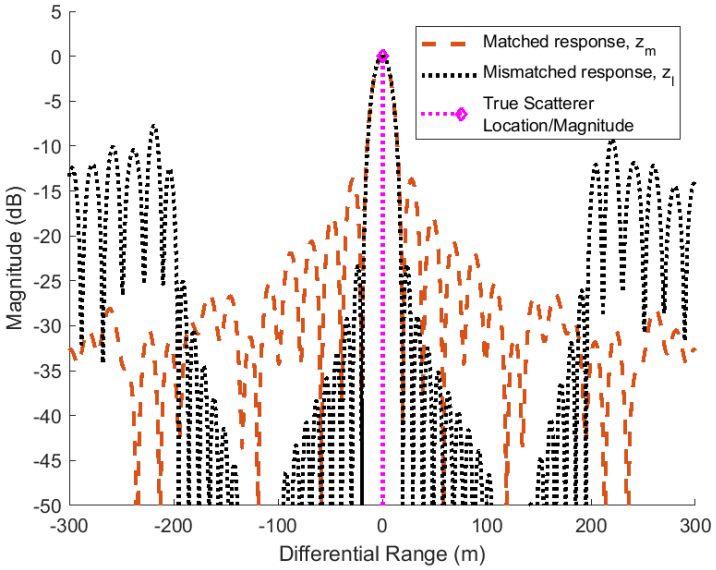

(a) Zoomed impulse response for center pulse

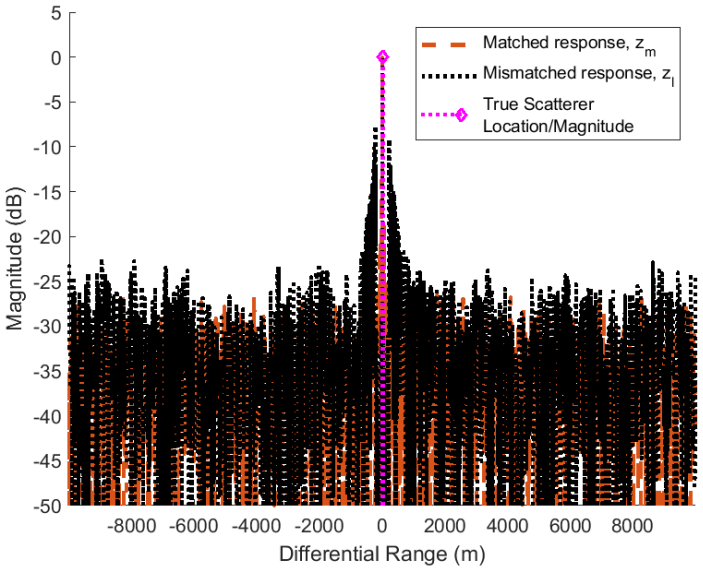

(b) Full impulse response for center pulse

Figure 20: The zoomed impulse response (a) and full impulse response for a matched filter and MLSMMF with narrow rectangular weights for an SNR of ∞ using the OFDM signal parameters specified in Chapter II.

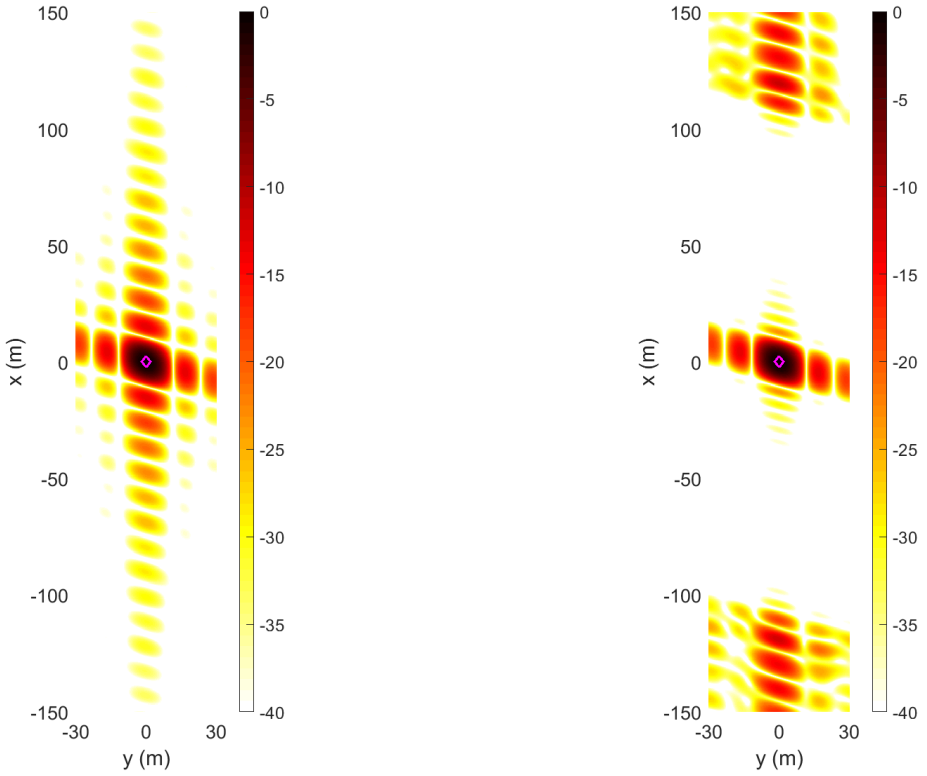

(a) PSF formed from Matched Filter

(b) PSF formed from MLSMMF

Figure 21: PSFs formed using a matched filter (a) and MLSMMF (b) with narrow rectangular weights for an SNR of ∞ using the OFDM signal parameters specified in Chapter II.

4.4.4 Moderate Noise, SNR = 0 dB, Narrow Rectangular Weighting Vector

For completion, this example extends the narrow rectangular weighting example to a noisy environment with an SNR of 0 dB. Figure 22a shows a typical zoomed in response formed from this narrow rectangular weighted MLSMMF compared against the corresponding matched filter response for an noiseless signal. The full response is shown in Figure 22b. In the noisy environment, the ISLR computed over the inner 2 percent of the range profile for this narrow rectangular weighting vector is 1.89 dB, compared to 15.67 dB for the uniform weighted vector and 5.30 dB for the matched filter.

The image formed over the 2 degree aperture is shown in Figure 23a for the matched filter and in Figure 23b for the MLSMMF. The ISLR_{PSF} for the MLSMMF is 14.92 dB while the ISLR_{PSF} of the matched filter is 15.57 dB.

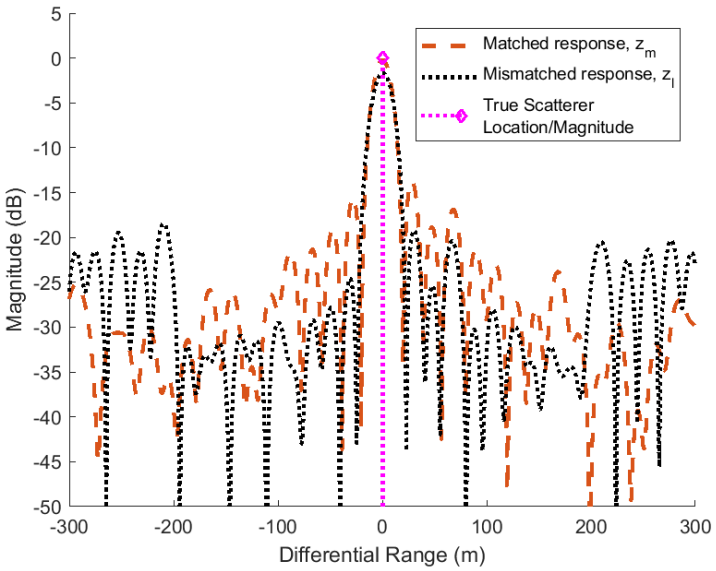

(a) Zoomed impulse response for center pulse

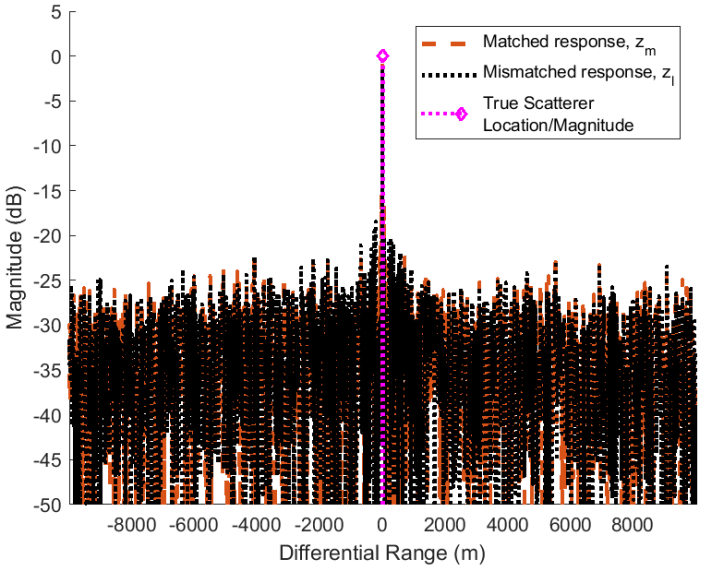

(b) Full impulse response for center pulse

Figure 22: The zoomed impulse response (a) and full impulse response for a matched filter and MLSMMF with narrow rectangular weights for an SNR of 0 dB using the OFDM signal parameters specified in Chapter II.

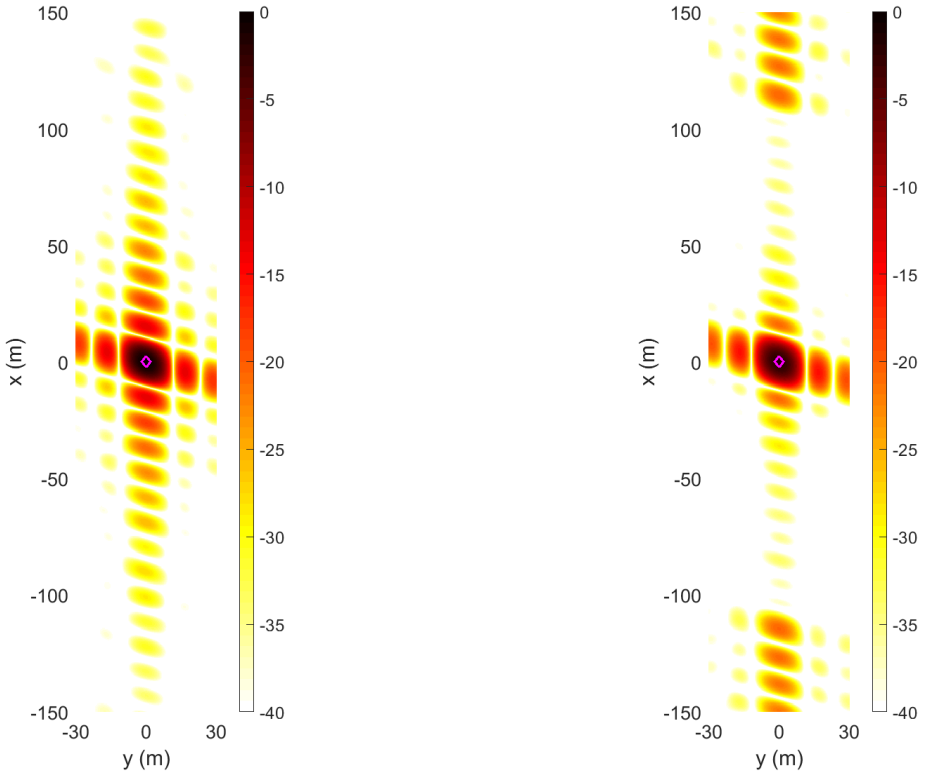

(a) PSF formed from Matched Filter

(b) PSF formed from MLSMMF

Figure 23: PSFs formed using a matched filter (a) and MLSMMF (b) with narrow rectangular weights for an SNR of 0 dB using the OFDM signal parameters specified in Chapter II.

4.4.5 Single Target Summary for Different Weighted MLSMMFs

The results from the previous examples demonstrating various weighting vectors are summarized here. The results for the noiseless cases are shown in Table 4. The results for the SNR = 0 dB cases are shown in Table 5. Each filter had its ISLR_{IR} calculated over the entire range profile, the center 20 percent of the range profile, and the center 2 percent of the range profile so that performance can be compared between each filter.

As shown previously, the uniform MLSMMF shows superior performance to the matched filter. From the tables below, this is true at each of the range intervals considered. The wide rectangular weighted MLSMMF was introduced to maximize

performance over the center 20 percent of the range profile. To this end, in the noiseless case it had an ISLR_{IR} over the center 20 percent of the range profile of -0.96 dB in the noiseless case, a significant improvement from the uniform weighted MLSMMF. This performance gain indicates that given a relatively confined scene, the wide rectangular weighting vector is capable of further reduction of sidelobes.

The narrow rectangular weighting vector was used as an example to show the limitations of a rectangular weighting vector. With the greatly reduced window size, performance was improved over the uniform case in a small range swath, but large sidelobes occuring downrange make use of the weighting scheme impractical. Also worth noting is that the wide rectangular weighted MLSMMF actually had a superior ISLR_{IR} over the center 2 percent of the range profile for the noiseless case. This is possible because minimizing the mean squared error between the mismatch response $\mathbf{z}_l$ and the ideal response $\mathbf{z}_i$ is slightly different than optimizing the ISLR_{IR}.

Table 4: Summary of ISLR over various ranges for each filter at an SNR = ∞

Filter Type	ISLR_{IR}	ISLR_{IR} (center 20%)	ISLR_{IR} (center 2%)	ISLR_{PSF}
Matched Filter	27.59	15.68	4.86	15.24
Uniform MLSMMF	20.86	8.12	0.03	11.74
Wide MLSMMF	37.03	-0.96	-3.72	9.22
Narrow MLSMMF	30.35	20.55	-2.67	16.15

Table 5: Summary of ISLR over various ranges for each filter at an SNR = 0 dB

Filter Type	$ISLR_{IR}$	$ISLR_{IR}$ (center 20%)	$ISLR_{IR}$ (center 2%)	$ISLR_{PSF}$
Matched Filter	30.24	18.08	5.30	15.57
Uniform MLSMMF	28.22	15.67	2.08	12.92
Wide MLSMMF	29.16	14.79	1.91	12.78
Narrow MLSMMF	31.14	19.60	1.89	14.92

4.5 Multiple Target Scenes

In this section, scenes will evolve beyond a single point target at the origin. In the first example, a set of point targets scattered around the scene is used to show how the sidelobe interactions of multiple targets appear in the image domain for each filter. The second example, a simple clutter environment will be used to demonstrate what effects are caused on the MLSMMF.

4.5.1 Multiple Point Targets

In this example, 6 point targets with various reflectivities are placed throughout the scene. The positions and reflectivities of these targets are listed in Table 6.

Table 6: Position and reflectivities of targets used in multi-target scenes.

Object Number	x (m)	y (m)	Reflectivity (dB)
1	-75	0	0
2	75	0	0
3	0	0	-15
4	117	0	-25
5	55	17	-25
6	120	25	-25

The uniform, wide rectangular, and narrow rectangular weighted MLSMMFs will be evaluated against the matched filter in this section using the same set of noisy signals to demonstrate which filter, if any, is likely to improve target identification. An SNR of 0 dB will be used throughout this example.

A typical response formed from both a matched filter and the uniform weighted MLSMMF for the same signal is shown in Figure 24a. The image formed over the 2 degree aperture is shown in Figure 24b for the matched filter and in Figure 24c for the MLSMMF.

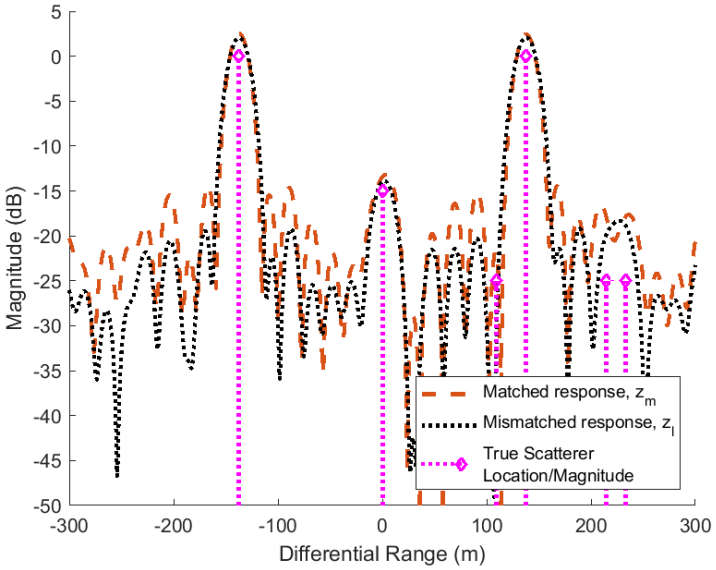

(a) Zoomed filter response for center pulse

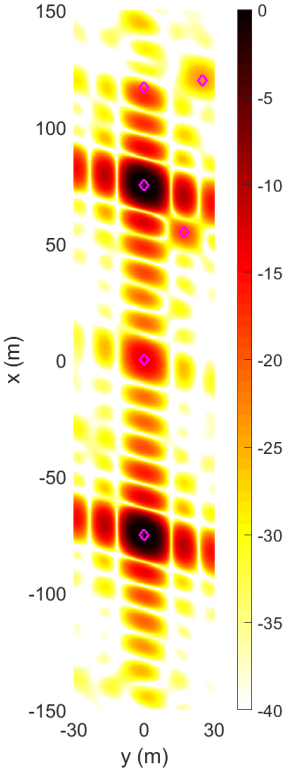

(b) Image formed from Matched Filter

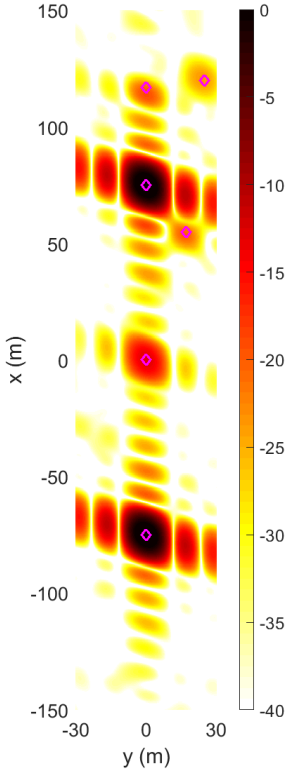

(c) Image formed from MLSMMF

Figure 24: The filter response (a) and images formed using a matched filter (b) and MLSMMF (c) with uniform weighting for an SNR of 0 dB using the OFDM signal parameters specified in Chapter II.

Object 3, located at the origin, is placed in between the dominant scatterers of Objects 1 and 2. In the matched filter image, Object 3 is of similar magnitude to the nearby sidelobes of Objects 1 and 2, and is only evident because of the wider mainlobe. In the MLSMMF image however, the sidelobes from Objects 1 and 2 are suppressed enough such that Object 3 is the brightest object in its relative area. Similar arguments can be made for Objects 4 and 5, whose magnitudes are more dominant in their relative areas in the MLSMMF image.

The motivation of reducing sidelobes as stated previously, is to help identify smaller targets in the sidelobes of larger targets. To this end, the MLSMMF does help the smaller objects dominate their respective locations by suppressing the sidelobes of other objects. This fact helps make the case that for some target identification processes, the MLSMMF may be more likely to identify these smaller objects.

Similar images are also formed for the wide rectangular weighted MLSMMF and narrow rectangular weighted MLSMMF.

A typical response formed from both a matched filter and the wide rectangular weighted MLSMMF for the same signal is shown in Figure 25a. The image formed over the 2 degree aperture is shown in Figure 25b for the matched filter and in Figure 25c for the MLSMMF. The results are similar to that of the uniform case with the argument being made that the smaller targets are more likely to be identified in the MLSMMF image than in the matched filter image.

A typical response formed from both a matched filter and the narrow rectangular weighted MLSMMF for the same signal is shown in Figure 26a. The image formed over the 2 degree aperture is shown in Figure 26b for the matched filter and in Figure 26c for the MLSMMF. In this case, because of the fact that each target blurs everything down range more than approximately 100 meters from it, the image is considerably blurred at the top and bottom, making identification of Object 4 impossible. As

mentioned earlier, for a rectangular weighting scheme to work effectively, the scene must be sufficiently contained. In this case, the scene is too spread out for the extreme amount of windowing used.

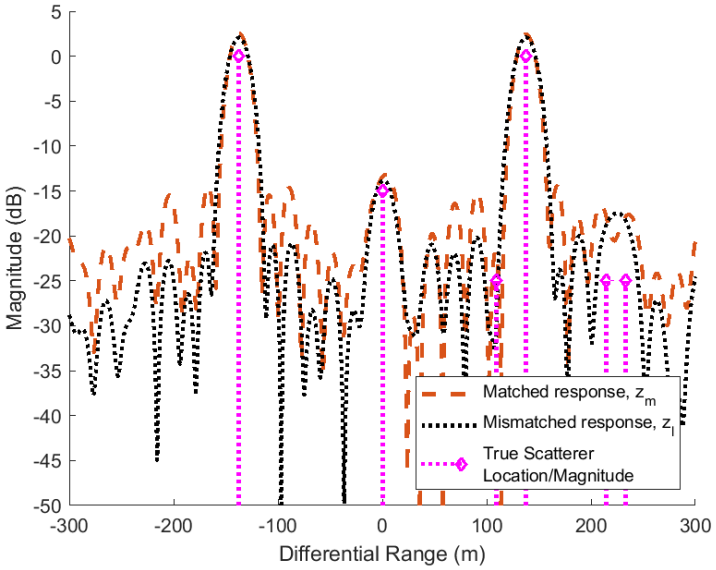

(a) Zoomed filter response for center pulse

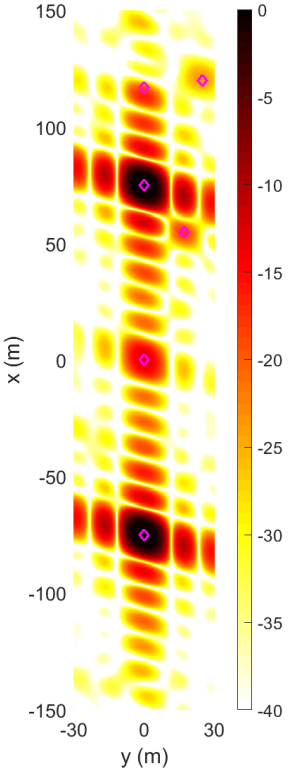

(b) Image formed from Matched Filter

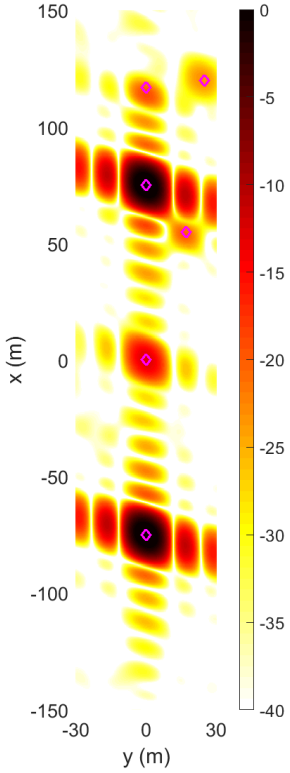

(c) Image formed from MLSMMF

Figure 25: The filter response (a) and images formed using a matched filter (b) and MLSMMF (c) with wide rectangular weighting for an SNR of 0 dB using the OFDM signal parameters specified in Chapter II.

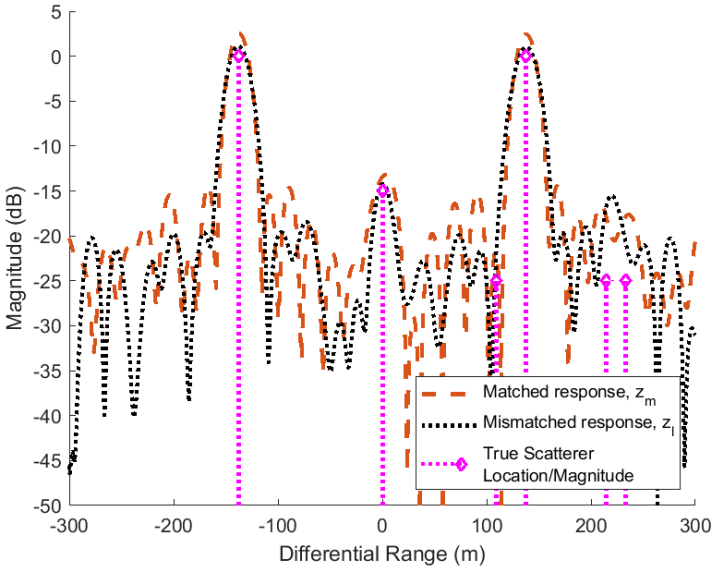

(a) Zoomed filter response for center pulse

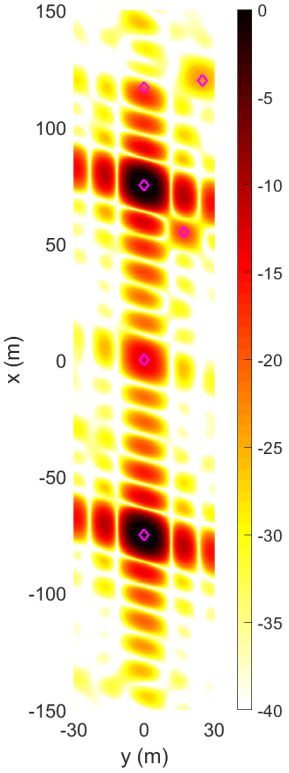

(b) Image formed from Matched Filter

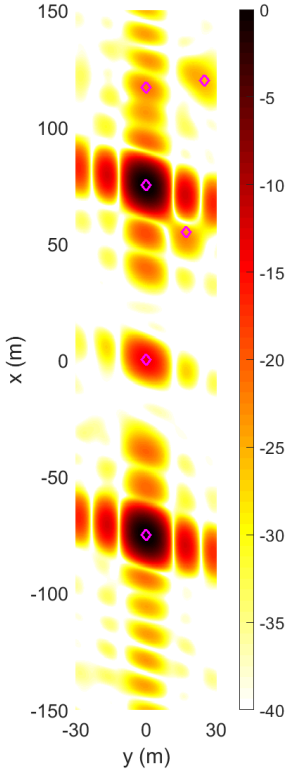

(c) Image formed from MLSMMF

Figure 26: The filter response (a) and images formed using a matched filter (b) and MLSMMF (c) with narrow rectangular weighting for an SNR of 0 dB using the OFDM signal parameters specified in Chapter II.

4.5.2 Clutter

In this section, a scene comprised of the same 6 objects as the previous example will be used, but with the addition of clutter as well. In this example clutter will be simulated by adding a scatterer every 2 meters in range and every 2 meters in cross-range. The reflectivities of the clutter scatterers have a Gaussian distribution with a mean of 0.015 and a standard deviation of 0.004. This corresponds to the most significant clutter cells having reflectivities of approximately -30 dB.

A typical response formed from both a matched filter and the uniform weighted MLSMMF for the same signal and clutter is shown in Figure 27a. The image formed over the 2 degree aperture is shown in Figure 27b for the matched filter and in Figure 27c for the MLSMMF. It is evident from the images that the sidelobes are of roughly the same proportions as previous examples, although the scene itself is considerably more complicated. The 6 well defined objects are harder to see amongst the clutter and neither filter technique suppresses the clutter. This result is expected, since a filter is only designed for a single target, and clutter can be thought of as a collection of targets spanning the scene.

This section is limited to a single example simply to show that the effects of clutter can not be compensated for with filter design.

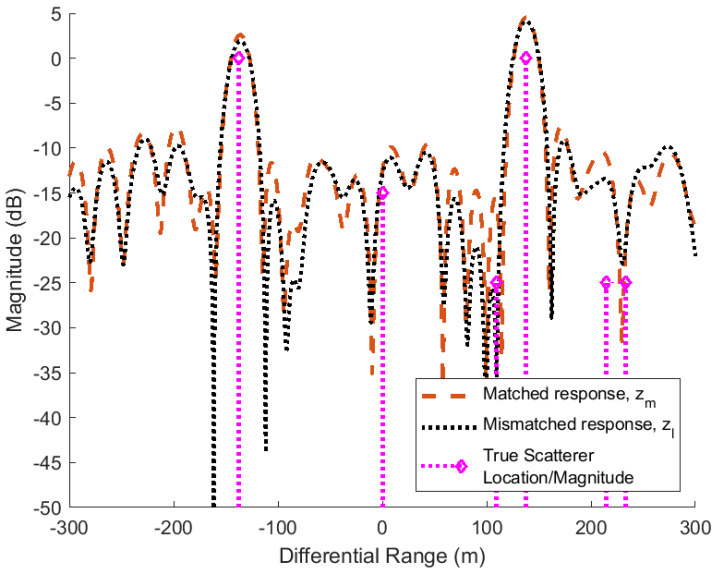

(a) Zoomed filter response for center pulse

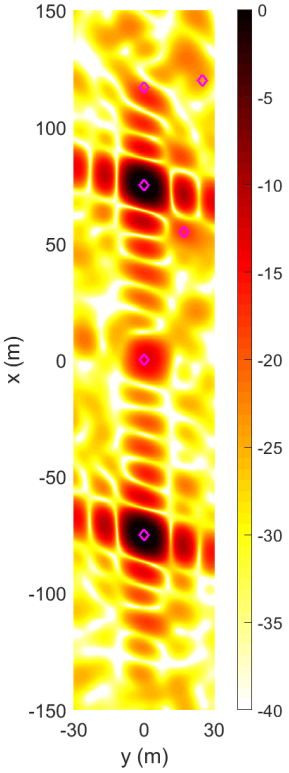

(b) Image formed from Matched Filter

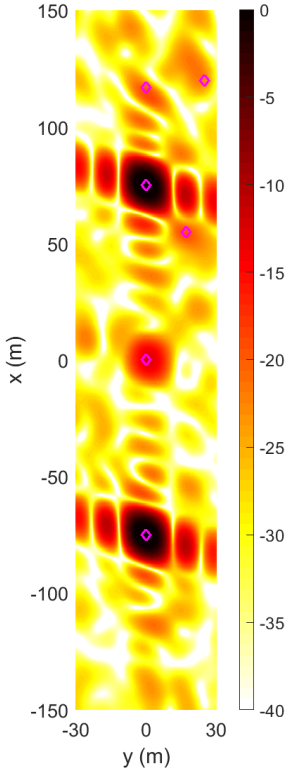

(c) Image formed from MLSMMF

Figure 27: The filter response (a) and images formed using a matched filter (b) and MLSMMF (c) with uniform weighting for an SNR of 0 dB using the OFDM signal parameters specified in Chapter II.

4.6 Noise Compensation Term Sensitivity

In this section, the sensitivity of the noise compensation term, $\mathbf{A}$, in (32) will be evaluated. Because the noise compensation term is dependent on the expected noise power, P_n, any error in the noise power measurement will lead to loss in filter performance. For the MLSMMF to be sufficiently robust, this loss in performance will ideally be small when the expected noise power deviates from the actual noise power.

To evaluate its sensitivity, the noise compensation term, $\mathbf{A}$, will be modified by various scale factors before forming the MLSMMF. This scaling is analogous to incorrectly estimating the noise power by the same scale factor. In each case however, the additive noise is of equal power, producing a signal with an SNR = 0 dB. The change in the ISLR_{IR} for various scale factors on $\mathbf{A}$ is listed in Table 7. The matched filter for the given SNR of 0 dB had an ISLR_{IR} of 30.24 dB while the properly compensated MLSMMF had a ISLR_{IR} of 28.22 dB. Scaling the noise compensation term by modest amounts has little effect on the sidelobe MLSMMF of the MLSMMF. When $\mathbf{A}$ is overestimated or underestimated by a factor of 2, the ISLR_{IR} degrades by less than 0.1 dB. Even when the noise power estimation is off by a factor of 100, the ISLR_{IR} degrades by only about 1 dB, forming a filter that still has better sidelobe suppression than the matched filter.

These results help show that the formulation of the noise compensation term in (32) does create an optimal filter with the best ISLR_{IR}, however, even large error in estimating the noise power is tolerable with only a small drop in performance.

Table 7: ISLR_{IR} for various uniform MLSMMFs with scaled noise compensation terms and an SNR = 0 dB.

Filter Type	ISLR_{IR}
Matched Filter	30.24
MLSMMF, **A** scaled by 0	39.99
MLSMMF, **A** scaled by 0.001	32.15
MLSMMF, **A** scaled by 0.01	29.16
MLSMMF, **A** scaled by 0.1	28.62
MLSMMF, **A** scaled by 0.5	28.27
MLSMMF, **A** scaled by 1	28.22
MLSMMF, **A** scaled by 2	28.30
MLSMMF, **A** scaled by 10	28.82
MLSMMF, **A** scaled by 100	29.25
MLSMMF, **A** scaled by 1000	29.31

4.7 Comparison to Phase History Windowing

In this section, the sidelobe MLSMMF performance of the MLSMMF will be compared to the technique of phase history windowing. As described in Chapter II, the phase history of each pulse can have a window applied to it which helps reduce the sidelobes in the response further from the target location. In this section, the window, $\mathbf{w}$, to be used will be a length NK Taylor window.

The signals and noise used for simulation in this section are the same as the ones

used in Section 4.3.3. This section will apply phase history windowing to both the matched filter and the MLSMMF and compare the results to those in Section 4.3.3.

A typical response formed from both a matched filter and the MLSMMF for the same signal with phase history windowing is shown in Figure 28a. The accompanying plot without phase history windowing was depicted previously in Figure 14a. Averaged over 41 different waveforms, the ISLR_{IR} of the MLSMMF with phase history windowing is 27.87 dB while the ISLR_{IR} of the matched filter with phase history windowing is 29.72 dB, both of which are improvements of approximately 0.5 dB to their non-windowed counterparts.

The image formed over the 2 degree aperture is shown in Figure 28b for the matched filter and in Figure 28c for the MLSMMF. The accompanying images without phase history windowing were depicted previously in Figure 14b and Figure 14c. While the sidelobes are noticeably reduced with phase history windowing, it is also evident that more mainlobe spreading has occurred due to the windowing.

Table 8 lists the resulting metrics of this section and Section 4.3.3. The figures in the table show that phase history windowing is an additional method of reducing sidelobes in the response, although similar to the MLSMMF, it also degrades the range resolution. Phase history windowing however is an independent process from the type of filter used however, so both can be used in conjunction when range resolution loss is of less concern than sidelobe MLSMMF.

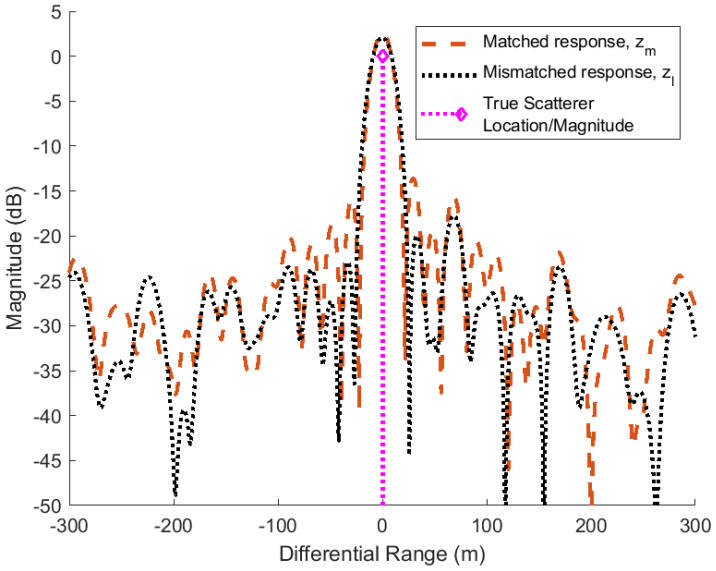

(a) Zoomed impulse response for center pulse

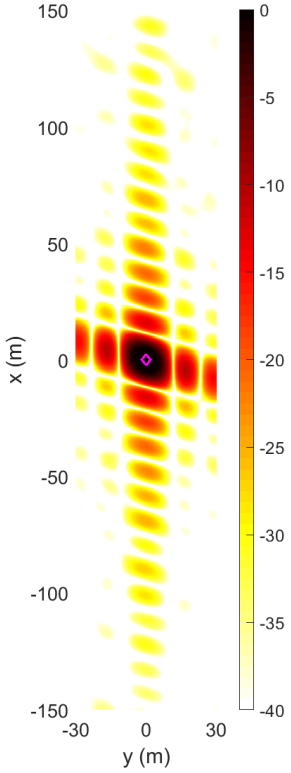

(b) PSF formed from Matched Filter

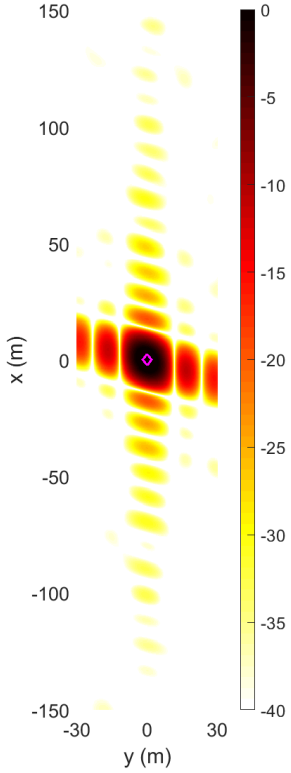

(c) PSF formed from MLSMMF

Figure 28: The impulse response (a) and PSFs formed using a matched filter (b) and MLSMMF (c) with uniform weighting for an SNR of 0 dB using phase history windowing and the OFDM signal parameters specified in Chapter II.

Table 8: ISLR_{IR}, ISLR_{PSF} and range resolution for matched filters and MLSMMFs with and without phase history windowing and an SNR = 0 dB.

Filter Type	ISLR_{IR}	ISLR_{PSF}	ρ_u
Matched Filter	30.24	15.57	9.30
Matched Filter with PHW	29.72	14.18	9.93
MLSMMF	28.22	12.92	10.40
MLSMMF with PHW	27.87	11.98	11.03

V. Conclusions

5.1 Key Conclusions

The results in Chapter IV indicate a number of differences between the matched filter, traditional LSMMF, and the MLSMMF derived in Chapter III. Notable findings include:

- Signal oversampling improves mismatch filter performance and is necessary for imaging applications but requires a new definition of the ideal filter response. In the absence of noise, the LSMMF with the modified ideal response is able to improve the ISLR across the filter response by approximately 6.7 dB.

- The traditional LSMMF even with the new ideal filter response is unable to cope with signal noise. However, the addition of a diagonal weighting matrix in the MLSMMF dependent on the noise power in the environment optimizes performance in noisy environments. The proportional improvement in ISLR decreases as noise levels increase.

- The MLSMMF technique increases the mainlobe width of the collection by 13.5 to 22 percent, depending on the oversampling rate, reducing range resolution by the same proportion.

- Even with significantly degraded SNRs, the MLSMMF noticeably decreases sidelobes in the response compared to that of the matched filter and produces cleaner images.

- Rectangular weights can be used to significantly increase sidelobe suppression in a reduced area. However, this method increases distant sidelobes to large levels causing scatterers to blur areas distant from them. Scenes with large

scatterers or clutter far from scene center are incompatible with this weighting technique.

- The MLSMMF only affects the sidelobes of a target response and does not provide any clutter rejection. Sidelobes from clutter are also reduced however, which may add some benefit over the matched filter in scenes with large amounts of clutter.

- Changes in the magnitude of the noise compensation term in the MLSMMF exhibit only a small reduction in sidelobe suppression. This indicates only a rough approximation of the noise power in the environment is required and that fluctuating noise levels will cause little degradation in performance.

- Mismatched filtering as a sidelobe suppression can be used along with other methods such as phase history windowing to achieve compound effects. Both of these methods increase mainlobe width however, so significant resolution losses will occur.

- Sidelobe suppression from the MLSMMF occurs only in the range dimension and not in the cross-range dimension. Sidelobe suppression in the cross-range dimension can be achieved when paired with other techniques such as phase history windowing.

5.2 Significance of the Research

Using the MLSMMF defined in Chapter III, significant sidelobe suppression is achieved compared to that of the matched filter for any given noise environment. While performance is best in no noise and low noise environments, superior performance is achieved at all SNRs unlike the traditional LSMMF which is unsuitable for applications with additive noise. The superior sidelobe suppression of the MLSMMF

reduces the odds of a smaller target being concealed within the sidelobes of a larger target at the cost of a small amount of mainlobe energy loss and spreading. Because of this limitation, the MLSMMF method is best utilized in situations where there are a multitude of scatterers spreading over several orders of magnitude in reflectivity. Application is also restricted to scenarios where processing time is of little concern, due to the slow processing time of forming the coefficients of the MLSMMF.

5.3 Future Studies

The results of this work could be extended by:

- Considering more complex scenes with additional transmitters. Multistatic effects caused from signals with different parameters or structures have not been considered.
- Set up a scene with more objects of varying reflectivities to more explicitly show the benefits of sidelobe suppression.
- Derive more concise metrics to evaluate image quality and range profile quality.
- Further modify the form of the MLSMMF to further improve sidelobe suppression. Changes may include a more rigorous definition of the ideal filter response for oversampled signals to reduce resolution loss.

Bibliography

1. M. H. Ackroyd and F. Ghani, "Optimum mismatched filters for sidelobe suppression," *IEEE Transactions on Aerospace and Electronic Systems*, vol. 9, no. 2, pp. 214–218, March 1973.

2. J. M. Baden and M. N. Cohen, "Optimal peak sidelobe filters for biphase pulse compression," in *IEEE Int'l Conf. on Radar*, May 1990, pp. 249–252.

3. K. R. Griep, J. A. Ritcey, and J. J. Burlingame, "Design of mismatched filters for pulse compression in a multiple user sonar ranging system," in *Proceedings of 27th Asilomar Conference on Signals, Systems and Computers*, Nov 1993, pp. 1111–1115 vol.2.

4. A. J. Zejak, I. S. Simic, Z. T. Golubicic, and A. Petrovic, "Mismatched compression filter for improved radar range resolution," in *6th IEEE Int'l Conf. on Electronics, Circuits and Systems*, vol. 2, Sep. 1999, pp. 733–736 vol.2.

5. A. J. Zejak, E. Zentner, and P. B. Rapajic, "Doppler optimised mismatched filters," *Electronics Letters*, vol. 27, no. 7, pp. 558–560, March 1991.

6. S. D. Blunt and K. Gerlach, "Adaptive pulse compression via MMSE estimation," *IEEE Transactions on Aerospace and Electronic Systems*, vol. 42, no. 2, pp. 572–584, April 2006.

7. M. S. Davis and A. D. Lanterman, "Minimum integrated sidelobe ratio filters for MIMO radar," *IEEE Transactions on Aerospace and Electronic Systems*, vol. 51, no. 1, pp. 405–416, January 2015.

8. D. Henke, P. McCormick, S. D. Blunt, and T. Higgins, "Practical aspects of optimal mismatch filtering and adaptive pulse compression for FM waveforms," in *IEEE Radar Conference*, May 2015, pp. 1149–1155.

9. M. A. Richards, J. A. Scheer, and W. A. Holm, Eds., *Principles of Modern Radar, Vol I: Basic Principles*. New Jersey: SciTech Publishing, 2010.

10. M. Soumekh, *Synethic Aperture Radar Signal Processing with MATLAB Algorithms*. New Jersey: Wiley-Interscience, 1999.

11. C. Jakowatz, D. Wahl, P. Eichel, D. Ghiglia, and P. Thompson, *Spotlight-Mode Synthethic Aperture Radar: A Signal Processing Approach*. Boston, MA: Kluwer Academic Publishers, 1996.

12. J. E. Palmer, H. A. Harms, S. J. Searle, and L. M. Davis, "Dvb-t passive radar signal processing," *IEEE Transactions on Signal Processing*, vol. 61, no. 8, pp. 2116–2126, April 2013.

13. S. Treitel and E. A. Robinson, "The design of high-resolution digital filters," *IEEE Transactions on Geoscience Electronics*, vol. 4, no. 1, pp. 25–38, June 1966.

14. C. Sahin, J. G. Metcalf, and S. D. Blunt, "Filter design to address range sidelobe modulation in transmit-encoded radar-embedded communications," in *IEEE Radar Conference*, May 2017, pp. 1509–1514.

15. J. M. Kempf and J. A. Jackson, "A modified least-squares mismatched filter for use in radar applications with additive noise," in *IEEE International Radar Conference*, April 2020.

16. S. D. Blunt, K. Gerlach, and T. Higgins, "Aspects of radar range superresolution," in *IEEE Radar Conference*, April 2007, pp. 683–687.

Acronyms

ISLR integrated sidelobe ratio. ix, 19, 20, 21, 22, 30, 31, 33, 35, 47, 49, 51, 54, 57, 60, 61, 75

LSMMF least-squares mismatched filter. vii, 2, 3, 4, 15, 17, 19, 24, 25, 27, 28, 31, 36, 41, 47, 75, 76

LTE Long-Term Evolution. 8

MLSMMF modified LSMMF. vi, vii, ix, 18, 19, 24, 30, 31, 32, 34, 35, 36, 38, 39, 40, 41, 42, 43, 44, 45, 46, 47, 48, 49, 50, 51, 52, 53, 54, 55, 56, 57, 58, 59, 60, 61, 62, 63, 64, 66, 67, 68, 69, 70, 71, 72, 73, 74, 75, 76, 77

OFDM orthogonal frequency-division multiplexing. v, ix, 3, 4, 7, 8, 9, 11, 20, 25, 27, 28, 30, 31, 34, 35, 40, 42, 44, 46, 50, 51, 53, 54, 56, 57, 58, 59, 63, 66, 67, 69, 73

PSF point spread function. v, ix, 21, 22, 23, 37, 39, 41, 43, 45, 47, 73

PSK phase shift keying. 7

QAM quadrature amplitude modulation. 7

SAR synthetic aperture radar. v, 1, 4, 5, 6, 7, 8, 13, 21, 26

SNR signal-to-noise ratio. vi, ix, 1, 15, 27, 28, 30, 31, 38, 40, 41, 42, 43, 44, 45, 46, 47, 48, 50, 51, 53, 54, 56, 57, 58, 59, 60, 61, 62, 63, 66, 67, 69, 70, 71, 73, 74, 75, 76

REPORT DOCUMENTATION PAGE

Form Approved
OMB No. 0704–0188

1. REPORT DATE *(DD–MM–YYYY)*	2. REPORT TYPE	3. DATES COVERED *(From — To)*
19–03–2020	Master's Thesis	Sept 2018 — Mar 2020

4. TITLE AND SUBTITLE

Mismatched Filter Effects On Synthetic Aperture Radar Image Quality Metrics

5a. CONTRACT NUMBER

5b. GRANT NUMBER

5c. PROGRAM ELEMENT NUMBER

6. AUTHOR(S)

Kempf, Jerrod M., Captain, USAF

5d. PROJECT NUMBER

5e. TASK NUMBER

5f. WORK UNIT NUMBER

7. PERFORMING ORGANIZATION NAME(S) AND ADDRESS(ES)

Air Force Institute of Technology
Graduate School of Engineering and Management (AFIT/EN)
2950 Hobson Way
WPAFB OH 45433-7765

8. PERFORMING ORGANIZATION REPORT NUMBER

AFIT-ENG-MS-20-M-030

9. SPONSORING / MONITORING AGENCY NAME(S) AND ADDRESS(ES)

Air Force Research Laboratory - Sensors Directorate
Dr. Braham Himed, AFRL/RYMD Division Research Fellow
2241 Avionics Circle, Bldg. 620, WPAFB, OH 45433
(937) 713-8124
Email: braham.himed@us.af.mil

10. SPONSOR/MONITOR'S ACRONYM(S)

AFRL/RYMD

11. SPONSOR/MONITOR'S REPORT NUMBER(S)

12. DISTRIBUTION / AVAILABILITY STATEMENT

DISTRIBUTION STATEMENT A:
APPROVED FOR PUBLIC RELEASE; DISTRIBUTION UNLIMITED.

13. SUPPLEMENTARY NOTES

This material is declared a work of the U.S. Government and is not subject to copyright protection in the United States.

14. ABSTRACT

Detection of targets across a wide dynamic range is an enduring challenge in radar. This work formulates a modified least-squares mismatched filter that greatly reduces these sidelobes in order to enable the detection of small radar cross section targets in the presence of considerably larger scatterers, increasing the dynamic range. Unlike previous mismatched filters, the proposed filter is applicable to noisy, oversampled signals with no requirements on signal structure. Range profiles and images are presented to demonstrate the superior sidelobe suppression of the modified least-squares mismatched filter in comparison to the commonly employed matched filter. Various weighting vectors are introduced to further increase sidelobe suppression for particular scene geometries. The modified mismatched filter created with the addition of a noise compensation term is shown to have superior sidelobe suppression to that of the matched filter across all signal-to-noise ratios, coming at the relatively low expense of a small degree of mainlobe energy loss and widening, as well as increased processing time.

15. SUBJECT TERMS

mismatched filters, least-squares, filter design, sidelobe suppression techniques, passive SAR

16. SECURITY CLASSIFICATION OF:			17. LIMITATION OF ABSTRACT	18. NUMBER OF PAGES	19a. NAME OF RESPONSIBLE PERSON
a. REPORT	b. ABSTRACT	c. THIS PAGE			Dr. J. A. Jackson, AFIT/ENG
U	U	U	UU	91	19b. TELEPHONE NUMBER *(include area code)* (937) 255-3636, ext 4678; julie.jackson@afit.edu